J. Mech. Phys. Solids 193 (2024) 105905

Contents lists available at ScienceDirect

Journal of the Mechanics and Physics of Solids

journal homepage: www.elsevier.com/locate/jmps

Eulerian rates of elastic incompatibilities applied to size-dependent hardening in finite torsion

M.B. Rubin [a], Lorenzo Bardella [b,*]

[a] Faculty of Mechanical Engineering, Technion-Israel Institute of Technology, 32000 Haifa, Israel
[b] Department of Civil, Environmental, Architectural Engineering and Mathematics, University of Brescia, Italy

ARTICLE INFO

Keywords:
Anisotropic elastic response
Elastic incompatibility
Elastic–inelastic
Eulerian formulation
Large deformation
Small-scale metal plasticity
Size-effect

ABSTRACT

Measures of rates of elastic incompatibilities are developed within an Eulerian framework for finite-deformation response of anisotropic elastic–inelastic materials. Such framework relies on the evolution of microstructural vectors. It is emphasized that the rates of incompatibilities, here denoted as R_{ij}, depend on the constitutive equation for the rate of inelasticity. For small strains and rotations, R_{ij} are equal to the negative of the components of the rate of Nye-Kröner's dislocation density tensor. In contrast to these small strain components, each R_{ij} is invariant under superposed rigid body motions such that it can be used independently in the constitutive equations to describe the material behavior. Specifically, in this work, R_{ij} provide a size-dependent enhancement to hardening that can increase or decrease during loading history, modeling the generation and annihilation of densities of geometrically necessary dislocations in metal plasticity. The application to the finite-deformation cyclic torsion of thin wires demonstrates the potential of this approach and the importance of the constitutive equation for the plastic spin rate both on the rotations of the microstructural vectors and on the predicted size-effect.

1. Introduction

Finite-deformation total strains are purely kinematic variables that measure deformation from a specified reference configuration to the current configuration. For example, a material point located at $\mathbf{X}$ in an arbitrary reference configuration at time $t = 0$ is deformed to its location $\mathbf{x}$ in the current configuration at time t by a one-to-one mapping

$$\mathbf{x} = \mathbf{x}(\mathbf{X}, t) \tag{1}$$

and the associated deformation gradient $\mathbf{F}$ is defined by

$$\mathbf{F} = \partial \mathbf{x} / \partial \mathbf{X} .$$

By definition, this mapping and the associated deformation gradient characterize a compatible deformation field from the reference configuration to the present configuration. Moreover, from an experimental point of view, Wilkinson et al. (2006) describe improvements in the analysis of electron backscatter diffraction (EBSD) patterns, which increase the accuracy of measuring small total distortional strains.

One question of compatibility arises when $\mathbf{F}$ is a specified function of $(\mathbf{X}, t)$ and it is not known if an associated compatible deformation field with a mapping of the form (1) exits. Yavari (2013) discusses the history of this problem for nonlinear elasticity

* Corresponding author.
E-mail addresses: mbrubin@tx.technion.ac.il (M.B. Rubin), lorenzo.bardella@ing.unibs.it (L. Bardella).

https://doi.org/10.1016/j.jmps.2024.105905
Received 26 May 2024; Received in revised form 3 September 2024; Accepted 7 October 2024
Available online 11 October 2024

and generalizes the solution for multiply connected regions. Here, attention is confined to simply connected regions for which the necessary and sufficient condition for a compatible mapping (1) to exist is that

$$\oint_C \mathbf{F}\mathrm{d}\mathbf{X} = \int_S \mathrm{Curl}(\mathbf{F})\mathbf{N}\mathrm{d}A = \mathbf{0}$$

for all closed paths C in the body, where Stoke's theorem is used to convert the line integral into an integral over the enclosed surface S. Moreover, Curl( ) is the curl operator with respect to $\mathbf{X}$, $\mathbf{N}$ is the unit normal to S, right-handed relative to the direction of integration on C, and $\mathrm{d}A$ is the reference area element on S. Assuming sufficient continuity, it follows that

$$\mathrm{Curl}(\mathbf{F}) = \mathbf{0} \tag{2}$$

at every point in the body.

In the finite-deformation Lagrangian formulation of constitutive equations for elastic–inelastic response, it is typical to use evolution equations for total and plastic deformation tensors (Bilby et al., 1957; Kröner, 1959; Green and Naghdi, 1965; Lee, 1969). In this formulation the elastic deformation tensor $\mathbf{F}_e$ can be defined as a function of the total deformation gradient $\mathbf{F}$ and a plastic deformation tensor $\mathbf{F}_p$ in the multiplicative form

$$\mathbf{F}_e = \mathbf{F}\mathbf{F}_p^{-1} .$$

Alternatively, Besseling (1966) proposed an evolution equation for $\mathbf{F}_e$ directly. In these Lagrangian formulations, $\mathbf{F}$ connects a reference configuration to the current configuration, $\mathbf{F}_p$ connects a reference configuration to an intermediate configuration, and $\mathbf{F}_e$ connects an intermediate configuration to the current configuration. On this basis, there have been several contributions (see, e.g., Kröner, 1959; Shizawa and Zbib, 1999; Acharya and Bassani, 2000; Cermelli and Gurtin, 2001; Starkey et al., 2020, and references therein) aiming at characterizing the incompatibility of the plastic deformation field and using it to model the effect of densities of geometrically necessary dislocations (GNDs) in metal plasticity (Ashby, 1970). However, Lagrangian formulations introduce arbitrariness of the choices of the reference and intermediate configurations as well as arbitrariness of the choices of the total and inelastic deformation measures tensor (Rubin, 2012). Therefore, in the Lagrangian framework, there are a number of options to discuss incompatibility depending, for instance, on the configuration on which the *net* Burgers vector is determined through a definition similar to Eq. with $\mathbf{F}$ being substituted with either $\mathbf{F}_p$ or $\mathbf{F}_e$ (Cermelli and Gurtin, 2001).

With regard to formulations of large deformation inelasticity, Eckart (1948) clearly states that the two following assumptions in the understanding of inelasticity are *false*:

(A1) The existence of a constant relaxed state.
(A2) The principle of relaxability-in-the-large, asserting that the strains in a solid can be completely relaxed by removing all external loads.

Eckart (1948) also states that "…Saint-Venant's conditions for the relaxibility-in-the-large are essentially identical with Riemann's geometric conditions". and "…if a small bit of the matter surrounding P is cut out of the larger object, then all strains in this bit will be relaxed, since it will have no forces acting on it". In the review of the origins of multiplicative expressions connecting total, elastic, and inelastic deformation measures, Sadik and Yavari (2017) note that this comment is similar to comments interpreting the "intermediate configuration", which is a basis for the multiplicative connections of total, elastic, and plastic deformations measures in many finite-plasticity theories.

Eckart (1948) seems to be the first one to emphasize that, since stress depends on elastic deformation, an evolution equation for elastic deformation can be proposed directly in terms of itself, the velocity gradient, and a measure of inelastic deformation rate. This formulation is Eulerian in the sense that it does not depend on choices of total or plastic deformation tensors, nor on reference and intermediate configurations. A similar formulation for polymeric liquids is proposed by Leonov (1976). Both formulations are valid for elastically isotropic response.

An Eulerian formulation of constitutive equations for the elastic–inelastic response of an elastically anisotropic material has been developed in (Rubin, 1994). This formulation introduces evolution equations for a right-handed triad $\mathbf{m}_i$ of linearly independent microstructural vectors of the forms

$$\dot{\mathbf{m}}_i = (\mathbf{L} - \mathbf{L}_p)\mathbf{m}_i , \tag{3}$$

where $\dot{(\ )}$ denotes the material time derivative, $\mathbf{L}$ is the total velocity gradient, and $\mathbf{L}_p$ is a general second-order tensor characterizing inelastic rate, which requires a constitutive equation. The microstructural vectors $\mathbf{m}_i$ characterize elastic deformations and orientation changes of anisotropic directions in the material from a zero-stress state. They also determine the Cauchy stress $\mathbf{T}$ in the current state. In particular, it is noted that when $\mathbf{L}_p$ vanishes, $\mathbf{m}_i$ deform like material line elements and the theory predicts anisotropic hyperelastic response. These microstructural vectors $\mathbf{m}_i$ are internal state variables, as defined by Onat (1968), that are assumed to be measurable in the current state. Specifically, it is assumed that the constitutive equation for stress $\mathbf{T}$ and the evolution equations for $\mathbf{m}_i$ can be used to determine $\mathbf{m}_i$ given local measurements of stress, which are known to be quite difficult. It is further specified that the Eulerian formulation relying on Eq. (3) is phenomenological and general, as it does not refer to any particular microstructure of the material.

It is emphasized that the Eulerian formulation of constitutive equations requires the constitutive equations to be functions of the values of state variables in the current state. This differs from an Eulerian representation of quantities in continuum mechanics. Specifically, the total deformation gradient $\mathbf{F}$ can be represented either in Lagrangian or in Eulerian forms but it is not admitted as

a state variable in the Eulerian formulation because it depends on an arbitrary specification of the reference configuration, which cannot be determined by experiments on the material in its current state for general elastic–inelastic deformations.

Typically, for a uniform homogeneous material, the elastic deformation from a uniform zero-stress state is compatible when the total applied deformation is homogeneous. However, inhomogeneous loading, in general, causes residual stresses when the external loads are removed. These residual stresses indicate that the elastic deformation field is no longer compatible. Thus, compatibility of the elastic deformation from a uniform zero-stress state is only a very special case of elastic–inelastic response.

The constitutive equation for stress is assumed to be invertible and is restricted so that $\mathbf{m}_i$ are orthonormal when the material is in a Reference Lattice State (RLS) with zero stress and reference temperature (Rubin, 1994). In the RLS, the metric

$$m_{ij} = \mathbf{m}_i \cdot \mathbf{m}_j \tag{4}$$

is equal to the Kronecker delta δ_{ij}. Consequently, measurements of stress and temperature determine $\mathbf{m}_i$ in the current state, which are initial conditions for integrating (3) by inverting the constitutive equation for the Cauchy stress. It is emphasized that, in contrast with total deformations, the elastic deformations and orientations of $\mathbf{m}_i$ are not purely kinematic variables since they depend on a constitutive equation for the inelastic deformation rate. In Eq. (4) and henceforth, $\cdot$ denotes the inner product.

Here, it is assumed that $\mathbf{m}_i$ are at least twice continuously differentiable, so jumps in elastic strain gradients, as analyzed for the linear theory by Fosdick and Royer-Carfagni (2020), are omitted. In this regard, it is noted that, in standard rate-independent elastic–plastic models with a yield function, imposing a consistency condition causes a discontinuous slope in a stress–strain curve at the onset of yielding, which is inconsistent with the assumed continuity of $\mathbf{m}_i$. However, viscoplastic models (e.g. Malvern, 1951; Perzyna, 1963; Bodner and Partom, 1972) and the smooth elastic–inelastic transition model in Hollenstein et al. (2013, 2015), for both rate-dependent and rate-independent responses, eliminate this discontinuous slope at the onset of yielding. Moreover, as measurement techniques improved, assumed shock discontinuities in metals were revealed as rapid continuous transition regions (Johnson and Barker, 1969). Thus, the continuity assumption on $\mathbf{m}_i$ may be physical even in nearly sharp transition regions.

The main objective of this paper is to propose Eulerian rates of elastic incompatibilities, on the basis of necessary and sufficient conditions for elastic incompatibility developed in Section 3, after fundamental kinematic definitions are provided in Section 2. In particular, in Section 4, the Eulerian rates of elastic incompatibilities, here denoted as R_{ij}, are defined as components of the current curl of the negative of the inelastic rate tensor relative to the distortional microstructural vectors $\mathbf{m}_i'$, which, differently from the $\mathbf{m}_i$, are insensitive to elastic dilatation.

Section 5 presents specific constitutive equations that use R_{ij} to predict size-dependent hardening. With respect to the literature on strain-gradient plasticity (SGP), the proposed theory is a lower-order one, as it does not involve higher-order balance equations nor higher-order boundary conditions (Niordson and Hutchinson, 2003). Although this surely limits the capability of the proposed theory, it is enough to reach the objectives of this investigation, which consist of demonstrating the potential of the proposed R_{ij} and emphasizing the role of the constitutive equation for the rate of inelasticity, with an accent on the plastic spin rate. In particular, this important aspect suggests the opportunity to directly use the rates of incompatibilities in constitutive equations for the time-evolution of the relevant fields such as the hardening variables, instead of time-integrating the rates of incompatibilities to obtain a primal kinematic variable (i.e., a Nye-Kröner-like tensor, Nye, 1953; Kröner, 1962) to be then employed in the constitutive equations (Rubin and Bardella, 2023). Again, this issue is typical of the Eulerian formulation of constitutive equations, while in the large-deformation Lagrangian framework one can directly write a finite Nye-Kröner-like tensor (Cermelli and Gurtin, 2001).

One of the key advantages of the direct use of R_{ij} in constitutive equations is that the R_{ij} components are invariant under superposed rigid body motions (SRBM), so they can be used independently in the constitutive equations to model the material behavior under study. For instance, they can be used to define measures of incompatibility allowing for full or partial recovery of the size-dependent hardening, towards accounting for both the nature of GNDs in metal plasticity (Ashby, 1970) and the dissipation associated with dislocations' motion (Needleman, 2024). These concepts are illustrated and discussed through the example of Section 6, dealing with the size-dependent response of thin metal wires subjected to finite-deformation cyclic torsion. Concluding remarks are offered in Section 7.

2. The elastic deformation gradient

The position vectors $\mathbf{X}$ and $\mathbf{x}$ can be expressed in terms of arbitrary convected coordinates θ^i such that

$$\mathbf{X} = \mathbf{X}(\theta^i)\,, \quad \mathbf{G}_i = \mathbf{X}_{,i} \equiv \partial \mathbf{X}/\partial\theta^i\,, \quad \mathbf{x} = \mathbf{x}(\theta^i, t)\,, \quad \mathbf{g}_i = \mathbf{x}_{,i}\,,$$

where a comma denotes partial differentiation with respect to θ^i and $\mathbf{G}_i$ and $\mathbf{g}_i$ are covariant base vectors in the initial and current configurations, respectively. Moreover, the contravariant base vectors $\mathbf{G}^i$ are defined by

$$\begin{aligned} &G^{1/2} = \mathbf{G}_1 \times \mathbf{G}_2 \cdot \mathbf{G}_3 > 0\,, \quad \mathbf{G}^1 = G^{-1/2}\mathbf{G}_2 \times \mathbf{G}_3\,, \quad \mathbf{G}^2 = G^{-1/2}\mathbf{G}_3 \times \mathbf{G}_1\,, \quad \mathbf{G}^3 = G^{-1/2}\mathbf{G}_1 \times \mathbf{G}_2\,, \\ &\mathbf{G}_i \cdot \mathbf{G}^j = \delta_i^j\,, \quad \mathbf{G}_j \otimes \mathbf{G}^j = \mathbf{I}\,, \end{aligned} \tag{5}$$

where $\times$ denotes the vector product, δ_i^j is the mixed Kronecker delta, and $\mathbf{I}$ is the second-order identity tensor. The reciprocal vectors $\mathbf{g}^i$ satisfy equations similar to (5) with $(G^{1/2}, \mathbf{G}_i)$ substituted by $(g^{1/2}, \mathbf{g}_i)$.

Since the microstructural vectors $\mathbf{m}_i$ in Eq. (3) are linearly independent, they can be defined so that the elastic dilatation J_e is positive

$$J_e = \mathbf{m}_1 \times \mathbf{m}_2 \cdot \mathbf{m}_3 > 0\,. \tag{6}$$

Moreover, the notion of elastic compatibility is Lagrangian in the sense that it requires a definition of elastic deformation between two configurations. Consequently, it is convenient to define the reciprocal vectors $\mathbf{M}^i$ and $\mathbf{m}^i$ in the initial configuration at $t = 0$ and in the current configuration at time t, by equations similar to (5). Then, the elastic deformation tensor $\mathbf{F}_m$ between the initial and current configurations satisfies the equations

$$\mathbf{F}_m = \mathbf{m}_s \otimes \mathbf{M}^s\,, \quad \dot{\mathbf{F}}_m = (\mathbf{L} - \mathbf{L}_p)\mathbf{F}_m\,, \quad \mathbf{F}_m(0) = \mathbf{I}\,, \tag{7}$$

where $\mathbf{a} \otimes \mathbf{b}$ denotes the tensor product between the two vectors $(\mathbf{a}, \mathbf{b})$. In this regard, it is noted that the metric m_{ij} in (4) measures elastic deformations from a zero-stress state, where $m_{ij} = \delta_{ij}$. The tensor $\mathbf{F}_m$ in (7) remains a measure of elastic deformation from the initial configuration even for a general initial configuration in an initial state with residual stresses.

3. Elastic incompatibility

3.1. A Nye-Kröner-like tensor

To discuss elastic incompatibility between the initial and current configurations, consider the Nye-Kröner-like elastic tensor $\boldsymbol{\alpha}_e$ (Nye, 1953; Kröner, 1962) relative to the initial configuration that satisfies the equations

$$\boldsymbol{\alpha}_e \equiv \mathrm{Curl}(\mathbf{F}_m) = -\mathbf{F}_{m,i} \times \mathbf{G}^i\,. \tag{8}$$

This is a two-point tensor that measures elastic incompatibilities from the initial configuration to the current configuration. Moreover, the material time derivative of $\boldsymbol{\alpha}_e$ is given by

$$\dot{\boldsymbol{\alpha}}_e = (\mathbf{L} - \mathbf{L}_p)\boldsymbol{\alpha}_e - (\mathbf{L} - \mathbf{L}_p)_{,i}\,\mathbf{F}_m \times \mathbf{G}^i\,. \tag{9}$$

It is noted that, by following Willis (1967), Acharya and Zhang (2015) define a Nye-Kröner-like tensor in terms of the curl of $\mathbf{F}_e^{-1}$ with respect to the current configuration, which is used to develop a mesoscopic theory of dislocation mechanics accounting for the conservation of the *net* Burgers vector.

3.2. A compatible deformation for nonlinear elasticity

A compatible deformation between the initial and current configurations for nonlinear elasticity $\mathbf{F}_m$ can be written in the alternative form

$$\mathbf{F}_m = \mathbf{g}_s \otimes \mathbf{G}^s\,, \tag{10}$$

with $\mathbf{L}_p = \mathbf{0}$. Therefore, by using the results

$$\mathbf{g}_{s,i} = \mathbf{g}_{i,s}\,, \qquad \mathbf{G}_{k,i} = \mathbf{G}_{i,k}\,, \qquad \mathbf{G}^s{}_{,i} = -\big(\mathbf{G}^s \cdot \mathbf{G}_{k,i}\big)\mathbf{G}^k\,,$$
$$\mathbf{L} = \dot{\mathbf{g}}_n \otimes \mathbf{g}^n\,, \quad \dot{\mathbf{g}}_{n,i} = \dot{\mathbf{g}}_{i,n}\,, \qquad \mathbf{g}^n{}_{,i} = -\big(\mathbf{g}^n \cdot \mathbf{g}_{k,i}\big)\mathbf{g}^k\,,$$

and substituting (10) into definition (8), it follows that

$$\boldsymbol{\alpha}_e = -\big[\mathbf{g}_{s,i} \otimes (\mathbf{G}^s \times \mathbf{G}^i) - \big(\mathbf{G}^s \cdot \mathbf{G}_{k,i}\big)\mathbf{g}_s \otimes (\mathbf{G}^k \times \mathbf{G}^i)\big] = \mathbf{0}.$$

Moreover, substituting (10) into the definition (9) with $\mathbf{L}_p = \mathbf{0}$ yields

$$\dot{\boldsymbol{\alpha}}_e = \mathbf{L}\boldsymbol{\alpha}_e - \big[\dot{\mathbf{g}}_{s,i} - \big(\mathbf{g}^n \cdot \mathbf{g}_{s,i}\big)\dot{\mathbf{g}}_n\big] \otimes \mathbf{G}^s \times \mathbf{G}^i = \mathbf{0}\,.$$

Assuming sufficient continuity, this shows that a compatible nonlinear elastic deformation remains compatible.

4. Eulerian rates of elastic incompatibilities for elastic–inelastic response

In order to motivate expressions for Eulerian rates of elastic incompatibilities for elastic–inelastic response, Eq. (9) is evaluated in the initial configuration, which is taken as the current configuration, with $(\mathbf{F}_m = \mathbf{I})$ and $(\mathbf{G}^i = \mathbf{g}^i)$, to obtain

$$\boldsymbol{\alpha}_e = \mathrm{Curl}(\mathbf{F}_m) = \mathbf{0}\,, \quad \dot{\boldsymbol{\alpha}}_e = \overset{\cdot}{\overline{\mathrm{Curl}(\mathbf{F}_m)}} = -\mathrm{curl}(\mathbf{L}_p)\,,$$

where use has been made of the fact that $\mathrm{curl}(\mathbf{L}) = \mathbf{0}$. From the result of previous Section 3.2, this implies that $-\mathrm{curl}(\mathbf{L}_p)$ is a second-order tensor measuring the evolution of the elastic incompatibility. This suggests defining the Eulerian rates of elastic incompatibility R_{ij} for finite deformations by the equations

$$R_{ij} = -\mathrm{curl}(\mathbf{L}_p) \cdot (\mathbf{m}'_i \otimes \mathbf{m}'_j)\,, \tag{11}$$

where the distortional microstructural vectors $\mathbf{m}'_i$ satisfy the equations

$$\mathbf{m}'_i = J_e^{-1/3}\mathbf{m}_i\,, \quad \dot{\mathbf{m}}'_i = (\mathbf{L}'' - \mathbf{L}''_p)\mathbf{m}'_i\,. \tag{12}$$

Here and henceforth, $(\,)''$ denotes the deviatoric part of a tensor, as

$$\mathbf{L}'' = \mathbf{L} - \frac{1}{3}\mathrm{tr}(\mathbf{L})\mathbf{I}\,, \tag{13}$$

where $\mathrm{tr}(\mathbf{A}) = \mathbf{A}\cdot\mathbf{I}$ denotes the trace of the second-order tensor $\mathbf{A}$. Also, the inner product between two second-order tensors $\mathbf{A}$ and $\mathbf{B}$ is such that $\mathbf{A}\cdot\mathbf{B} = \mathrm{tr}(\mathbf{A}\mathbf{B}^T)$. Moreover, taking the material derivative of (6) yields

$$\frac{\dot{J}_e}{J_e} = \dot{\mathbf{m}}_j\cdot\mathbf{m}^j = \mathrm{tr}(\mathbf{L}-\mathbf{L}_p) = \mathrm{tr}(\mathbf{D}-\mathbf{D}_p)\,, \quad \mathbf{D} = \frac{1}{2}(\mathbf{L}+\mathbf{L}^T)\,, \quad \mathbf{D}_p = \frac{1}{2}(\mathbf{L}_p+\mathbf{L}_p^T)\,, \tag{14}$$

where $\mathbf{D}$ and $\mathbf{D}_p$ are the total and the inelastic deformation rates, respectively. Moreover, for isochoric inelasticity

$$\mathrm{tr}(\mathbf{L}_p) = \mathrm{tr}(\mathbf{D}_p) = 0\,. \tag{15}$$

Next, using this result and the conservation of mass, the elastic dilatation can be rewritten in the form

$$J_e = \frac{\rho_z}{\rho}\,, \tag{16}$$

where ρ is the current mass density and ρ_z is its constant zero-stress value.

It is emphasized that the Nye-Kröner-like tensor in (8) measures incompatible deformations between the initial and current configurations, such as it is dependent on the choice of the initial configuration. In contrast, R_{ij} in Eq. (11) are Eulerian rates of elastic incompatibilities that are independent of arbitrary choices of reference and intermediate configurations as well as total and plastic deformation measures. Consequently, R_{ij} can be used in an Eulerian formulation of constitutive equations (Rubin, 2012, 2021). Moreover, it is observed that R_{ij} are highly nonlinear fields because they are quadratic in $\mathbf{m}_i'$, which depend on the loading history, as well as on $\mathbf{L}_p$.

4.1. Invariance under superposed rigid body motions

Under SRBM the quantities $(\mathbf{m}_i, \mathbf{m}^i, \mathbf{L}_p, \mathbf{g}_j, \mathbf{g}^j)$ transform to $(\mathbf{m}_i^+, \mathbf{m}^{i+}, \mathbf{L}_p^+, \mathbf{g}_j^+, \mathbf{g}^{j+})$, respectively, such that

$$\mathbf{m}_i^+ = \mathbf{Q}\mathbf{m}_i\,, \quad \mathbf{m}^{i+} = \mathbf{Q}\mathbf{m}^i\,, \quad \mathbf{L}_p^+ = \mathbf{Q}\mathbf{L}_p\mathbf{Q}^T\,, \quad \mathbf{g}_j^+ = \mathbf{Q}\mathbf{g}_j\,, \quad \mathbf{g}^{j+} = \mathbf{Q}\mathbf{g}^j\,, \tag{17}$$

where $\mathbf{Q}(t)$ is a proper orthogonal second-order tensor, function of time only,

$$\mathbf{Q}\mathbf{Q}^T = \mathbf{I}\,, \quad \det(\mathbf{Q}) = +1\,. \tag{18}$$

Then, using these expressions and the results in Appendix A, it follows that

$$\mathbf{F}_m^+ = \mathbf{Q}\mathbf{F}_m\,, \quad \mathrm{curl}^+(\mathbf{L}_p^+) = \mathbf{Q}\,\mathrm{curl}(\mathbf{L}_p)\,\mathbf{Q}^T\,,$$

so each component of the Eulerian rates of elastic incompatibilities R_{ij} in (11) is invariant under SRBM

$$R_{ij}^+ = -\mathrm{curl}^+(\mathbf{L}_p^+)\cdot(\mathbf{m}_i'^+\otimes\mathbf{m}_j'^+) = R_{ij}\,. \tag{19}$$

Thus, anisotropic constitutive equations can be arbitrary functions of R_{ij}.

4.2. Identification of R_{ij} with the negative rate of Nye-Kröner tensor for small strains and rotations

For small elastic deformations the vectors $\mathbf{m}_i$ and their reciprocals $\mathbf{m}^j$ can be expressed in the forms

$$\mathbf{m}_i = (\mathbf{I}+\mathbf{H}_e)\mathbf{e}_i\,, \quad \mathbf{m}^j = (\mathbf{I}-\mathbf{H}_e)^T\mathbf{e}_j\,,$$

where $\mathbf{H}_e$ is the small deformation elastic tensor, which can include both an elastic strain and an elastic rotation, and $\mathbf{e}_i$ is a fixed orthonormal triad of vectors. Moreover, the plastic tensor $\mathbf{H}_p$, which in general also includes a plastic strain and a plastic rotation, is defined by

$$\mathbf{H}_p = \mathbf{H}-\mathbf{H}_e\,,$$

where $\mathbf{H}$ is the total displacement gradient. Thus, the evolution Eq. (3) is approximated by

$$\dot{\mathbf{m}}_i = (\dot{\mathbf{H}}-\dot{\mathbf{H}}_p)\mathbf{e}_i\,, \quad \mathbf{L}_p = \dot{\mathbf{H}}_p\,.$$

Also, the evolution Eq. (11) is approximated by

$$R_{ij} = -\mathrm{curl}(\dot{\mathbf{H}}_p)\cdot(\mathbf{e}_i\otimes\mathbf{e}_j) = -(\dot{\mathbf{H}}_{p,s}\times\mathbf{e}_s)\cdot(\mathbf{e}_i\otimes\mathbf{e}_j) = -(\dot{H}^p_{mn},_s\,\mathbf{e}_m\otimes\mathbf{e}_s\times\mathbf{e}_n)\cdot(\mathbf{e}_i\otimes\mathbf{e}_j) = -\dot{H}^p_{in},_s\,\varepsilon_{snj}\,,$$
$$H^p_{ij} = \mathbf{H}_p\cdot(\mathbf{e}_i\otimes\mathbf{e}_j)\,, \quad \varepsilon_{snj} = \mathbf{e}_s\times\mathbf{e}_n\cdot\mathbf{e}_j\,,$$

which shows that R_{ij} is consistent with the negative of the time derivative of the Nye-Kröner tensor (Nye, 1953; Kröner, 1962), the latter being a measure of densities of GNDs that can be adopted to model size-effects in metal plasticity at the microscale (Ashby, 1970; Fleck and Hutchinson, 1997; Arsenlis and Parks, 1999). In particular, it can be shown that there are three rates of incompatibilities due to densities of screw dislocations characterized by

$$\{R_{11}\,, R_{22}\,, R_{33}\}\,, \tag{20}$$

and six rates of incompatibilities due to densities of edge dislocations characterized by

$$\{R_{12}\,, R_{13}\,, R_{21}\,, R_{23}\,, R_{31}\,, R_{32}\}\,. \tag{21}$$

5. A constitutive theory including elastic incompatibilities

5.1. The rate of material dissipation

In the purely mechanical theory the rate of material dissipation D is given by

$$D = \mathbf{T}\cdot\mathbf{D} - \rho\dot{\Sigma} \geq 0\,, \tag{22}$$

where $\mathbf{T}$ is the symmetric Cauchy stress and Σ is the strain energy function per unit mass.

5.2. Constitutive equations for general anisotropic elastic–inelastic response

The elastic distortional deformation metric m'_{ij} is defined as

$$m'_{ij} = \mathbf{m}'_i\cdot\mathbf{m}'_j$$

and satisfies the equation

$$\dot{m}'_{ij} = 2(\mathbf{m}'_i\otimes\mathbf{m}'_j - \frac{m'_{ij}}{3}\mathbf{I})\cdot(\mathbf{D}-\mathbf{D}''_p)\,.$$

Then, taking the strain energy Σ in the form

$$\Sigma = \Sigma(J_e, m'_{ij})$$

and specifying the stress $\mathbf{T}$ by

$$\mathbf{T} = -p\mathbf{I}+\mathbf{T}''\,,\quad p = -\rho J_e\frac{\partial\Sigma}{\partial J_e}\,,\quad \mathbf{T}'' = 2\rho\frac{\partial\Sigma}{\partial m'_{ij}}(\mathbf{m}'_i\otimes\mathbf{m}'_j - \frac{m'_{ij}}{3}\mathbf{I})\,, \tag{23}$$

the rate of material dissipation (22) for isochoric inelasticity (12)–(15) requires

$$\mathcal{D} = \mathbf{T}''\cdot\mathbf{D}_p \geq 0\,. \tag{24}$$

Also, the strain energy function is restricted so that $J_e = 1$ and $m'_{ij} = \delta_{ij}$ are consistent with a zero-stress state

$$\Sigma(1,\delta_{ij}) = 0\,,\quad \frac{\partial\Sigma}{\partial J_e}(1,\delta_{ij}) = 0\,,\quad \rho_z\frac{\partial\Sigma}{\partial m'_{ij}}(1,\delta_{ij}) = \frac{1}{2}\mu\delta_{ij}\,,$$

where μ is the zero-stress shear modulus in the isotropic case, otherwise μ can be one of the shear moduli characterizing the material anisotropy.

5.3. Constitutive equations for elastically isotropic elastic–inelastic response

5.3.1. The rate of inelasticity

For elastically isotropic response, the symmetric elastic distortional deformation $\mathbf{B}'_e$ is defined by

$$\mathbf{B}'_e = \mathbf{m}'_s\otimes\mathbf{m}'_s\,,\quad \mathbf{B}'^{-1}_e = \mathbf{m}^{s\prime}\otimes\mathbf{m}^{s\prime}\,. \tag{25}$$

Using the evolution Eq. (3), taking the time derivative of (25), and ensuring that $\mathbf{B}'_e$ remains unimodular ($\dot{\mathbf{B}}'_e\cdot\mathbf{B}'^{-1}_e = 0$) yields

$$\dot{\mathbf{B}}'_e = \mathbf{L}''\mathbf{B}'_e + \mathbf{B}'_e\mathbf{L}''^T - \Gamma\mathbf{A}_p\,,\quad \Gamma\mathbf{A}_p = \mathbf{L}_p\mathbf{B}'_e + \mathbf{B}'_e\mathbf{L}_p^T\,,\quad \mathbf{L}_p = \mathbf{L}''_p\,,$$

where the function $\Gamma\geq 0$ controls the rate of inelasticity. Moreover, $\mathbf{L}''_p$ is specified by

$$\mathbf{L}''_p = \mathbf{D}''_p + \mathbf{W}_p\,,\quad \mathbf{D}''_p = \frac{\Gamma}{2}\big(\mathbf{I} - \frac{3\mathbf{B}'^{-1}_e}{\mathrm{tr}(\mathbf{B}'^{-1}_e)}\big)\,,\quad \mathbf{W}_p = \frac{1}{2}(\mathbf{L}_p - \mathbf{L}_p^T)\,, \tag{26}$$

where $\mathbf{W}_p$ is the inelastic spin rate. It then can be shown that

$$\Gamma\mathbf{A}_p = \Gamma\big(\mathbf{B}'_e - \frac{3\mathbf{I}}{\mathrm{tr}(\mathbf{B}'^{-1}_e)}\big) + \mathbf{W}_p\mathbf{B}'_e + \mathbf{B}'_e\mathbf{W}_p^T\,,$$

which reduces to the form proposed in (Rubin and Attia, 1996) in the absence of inelastic spin. Also, in the absence of inelasticity, the evolution equation for $\mathbf{B}'_e$ causes it to be equal to the unimodular part $\mathbf{B}'$ of the left Cauchy–Green deformation tensor for all states if $\mathbf{B}'_e = \mathbf{B}'$ in any state.

Next, the inelastic spin is taken in the form proposed in (Lee and Rubin, 2021)

$$\begin{aligned}
&\mathbf{W}_p = \Omega_{12}(\mathbf{m}^{1\prime}\otimes\mathbf{m}^{2\prime} - \mathbf{m}^{2\prime}\otimes\mathbf{m}^{1\prime}) + \Omega_{31}(\mathbf{m}^{3\prime}\otimes\mathbf{m}^{1\prime} - \mathbf{m}^{1\prime}\otimes\mathbf{m}^{3\prime}) + \Omega_{23}(\mathbf{m}^{2\prime}\otimes\mathbf{m}^{3\prime} - \mathbf{m}^{3\prime}\otimes\mathbf{m}^{2\prime})\,,\\
&\Omega_{12} = \bar{\Omega}_{12}\chi_{12}\mathbf{D}''_p\cdot(\mathbf{m}'_1\otimes\mathbf{m}'_2) = \bar{\Omega}_{12}\chi_{12}\frac{\Gamma}{2}m'_{12}\,,\\
&\Omega_{31} = \bar{\Omega}_{31}\chi_{31}\mathbf{D}''_p\cdot(\mathbf{m}'_3\otimes\mathbf{m}'_1) = \bar{\Omega}_{31}\chi_{31}\frac{\Gamma}{2}m'_{31}\,,\\
&\Omega_{23} = \bar{\Omega}_{23}\chi_{23}\mathbf{D}''_p\cdot(\mathbf{m}'_2\otimes\mathbf{m}'_3) = \bar{\Omega}_{23}\chi_{23}\frac{\Gamma}{2}m'_{23}\,,
\end{aligned} \tag{27}$$

where $\bar{\Omega}_{12}, \bar{\Omega}_{31}, \bar{\Omega}_{23}$ are material constants controlling the rates of inelastic spin, and the functions $\chi_{12}, \chi_{31}, \chi_{23}$ are written in the forms

$$\chi_{12} = \frac{2}{\pi}\tan^{-1}\Big(\frac{m'_{22}-m'_{11}}{2m'_{12}}\Big)\,, \quad \chi_{31} = \frac{2}{\pi}\tan^{-1}\Big(\frac{m'_{33}-m'_{11}}{2m'_{13}}\Big)\,, \quad \chi_{23} = \frac{2}{\pi}\tan^{-1}\Big(\frac{m'_{33}-m'_{22}}{2m'_{23}}\Big)\,. \tag{28}$$

Note that in Eq. (28) the sign of χ_{31} has been changed relative to that in (Lee and Rubin, 2021). More importantly, in (Lee and Rubin, 2021) it has been shown that the form in Eqs. (27)–(28) for the inelastic spin rate can be calibrated to reproduce measured data for the orientation change of the principal directions of orthotropy for uniaxial stress loading at different angles relative to the rolling direction in sheet metal forming. The results of Section 6 demonstrate that inelastic spin plays a crucial role in determining the incompatibility of the elastic field, thus confirming previous findings in studies relying on Gurtin-type higher-order SGP theories (see, e.g., Bardella, 2009, comparing crystal and phenomenological SGPs, and Bardella and Panteghini, 2015, focusing on torsion). In contrast with the independent constitutive Eqs. (26) and (27) for $\mathbf{D}''_p$ and $\mathbf{W}_p$, respectively, in crystal plasticity the constitutive equation for $\mathbf{L}_p$ directly determines both $\mathbf{D}''_p$ and $\mathbf{W}_p$, as shown in Appendix B.

By using Eqs. (26) and (27), the evolution Eqs. (12) can be rewritten in the forms

$$\begin{aligned}
\dot{\mathbf{m}}'_1 &= \mathbf{L}''\mathbf{m}'_1 - \frac{\Gamma}{2}\Big(\mathbf{m}'_1 - \frac{3\mathbf{m}^{1\prime}}{\mathrm{tr}(\mathbf{B}'^{-1}_e)}\Big) + \Omega_{12}\mathbf{m}^{2\prime} - \Omega_{31}\mathbf{m}^{3\prime}\,,\\
\dot{\mathbf{m}}'_2 &= \mathbf{L}''\mathbf{m}'_2 - \frac{\Gamma}{2}\Big(\mathbf{m}'_2 - \frac{3\mathbf{m}^{2\prime}}{\mathrm{tr}(\mathbf{B}'^{-1}_e)}\Big) - \Omega_{12}\mathbf{m}^{1\prime} + \Omega_{23}\mathbf{m}^{3\prime}\,,\\
\dot{\mathbf{m}}'_3 &= \mathbf{L}''\mathbf{m}'_3 - \frac{\Gamma}{2}\Big(\mathbf{m}'_3 - \frac{3\mathbf{m}^{3\prime}}{\mathrm{tr}(\mathbf{B}'^{-1}_e)}\Big) + \Omega_{31}\mathbf{m}^{1\prime} - \Omega_{23}\mathbf{m}^{2\prime}\,.
\end{aligned} \tag{29}$$

5.3.2. A specific constitutive equation for the strain energy and stress

For elastically isotropic metals, Σ is specified by

$$\rho_z\Sigma = k\big[J_e - 1 - \ln(J_e)\big] + \frac{1}{2}\mu[\mathrm{tr}(\mathbf{B}'_e) - 3]\,, \tag{30}$$

where k is the zero-stress bulk modulus. In addition, using (16) and (25), the stress in Eq. (23) becomes

$$p = k\Big(\frac{1}{J_e} - 1\Big)\,, \quad \mathbf{T}'' = J_e^{-1}\mu\mathbf{B}''_e\,, \tag{31}$$

with the associated material dissipation

$$\mathcal{D} = \frac{1}{2}J_e^{-1}\mu\Gamma\,\mathrm{tr}(\mathbf{A}_p) \geq 0\,,$$

which is automatically satisfied since $\mathrm{tr}(\mathbf{A}_p) \geq 0$ (Rubin and Attia, 1996).

5.4. A smooth elastic–inelastic transition with length-dependent isotropic and directional hardening

A simple form of the smooth elastic–inelastic transition model for rate-independent response developed in Hollenstein et al. (2013, 2015) specifies Γ in (27) as

$$\Gamma = b_1\dot{\varepsilon}\langle g\rangle\,, \quad \dot{\varepsilon} = \sqrt{2/3}|\mathbf{D}''|\,, \quad g = 1 - \frac{y}{\gamma_e}\,, \quad \gamma_e = \sqrt{3/8}|\mathbf{B}''_e|\,, \tag{32}$$

where $b_1 > 0$ is a material parameter, $\dot{\varepsilon}$ is the equivalent total distortional deformation rate, g is a yield function, $|(\,)| \equiv \sqrt{(\,)\cdot(\,)}$ indicates the modulus, y is a hardening variable, γ_e is a measure of elastic distortional deformation, and the Macaulay brackets are defined by

$$\langle x\rangle = \max(x, 0)\,.$$

This model characterizes a smooth elastic–inelastic transition with overstress, where the transition becomes sharper and the amount of overstress becomes smaller with increasing b_1.

5.4.1. Isotropic hardening, including size-dependence

Since R_{ij} are invariant under SRBM, it is possible to establish a function of these components to obtain a field that can be used to enhance the hardening. Among several possibilities, this work considers the scalar field ξ defined by the evolution equation

$$\dot{\xi} = \ell\sum_{i=1}^{3}\sum_{j=1}^{3}R_{ij}\,, \tag{33}$$

where $\ell \geq 0$ is a characteristic material length. The variable ξ increases due to generation of defects while it decreases due to annihilation of defects.

In addition, consider a history-dependent hardening parameter Y defined by the evolution equations

$$Y = Y_H + Y_\ell\,, \quad \dot{Y}_H = \Gamma m_H(Y_{Hs} - Y_H)\,, \quad \dot{Y}_\ell = |\dot{\xi}|\big[m_\ell\langle Y_R - Y_\ell\rangle - m_r\langle Y_\ell - Y_R\rangle\big]\,, \quad Y_R = Y_{Rs}\,(1 - 10^{-|\xi|})^{n_R}\,, \tag{34}$$

along with annealed initial conditions

$$Y_H(t=0) = Y_{H0} \geq 0\,, \quad Y_\ell(t=0) = 0\,. \tag{35}$$

In Eq. (34), the constant $m_H \geq 0$ controls the rate of monotonic increase of size-independent hardening Y_H, from the initial value Y_{H0} towards its saturated value Y_{Hs}. In contrast, the size-dependent hardening variable Y_ℓ can increase or decrease towards its saturated value Y_R, which is a function of $|\xi|$, with a maximum value of Y_{Rs}. Also, the constant $m_\ell \geq 0$ controls the rate of increase of Y_ℓ, $m_r \geq 0$ controls the rate of decrease in Y_ℓ due to annihilation of defects, and $n_R \geq 0$ controls the shape of the function Y_R, that is, the orders of magnitude of size displaying an appreciable size-effect. Note that for $m_r = m_\ell$ the third relation in Eq. (34) becomes $\dot{Y}_\ell = |\dot{\xi}| m_\ell (Y_R - Y_\ell)$.

This direct use of ξ to determine size-dependent hardening parameters that increase the resistance to inelastic flow is very different from the use of the Nye-Kröner-like tensor in the Eulerian formulation of Rubin and Bardella (2023), such tensor being determined by integrating an evolution equation and being used to define a recoverable higher-order stress as in Gurtin (2004), in which, additionally, dissipative and energetic contributions due to the plastic spin were introduced for the first time in small-strain phenomenological SGP. With regard to the treatment of the plastic flow gradients, the present formulation is philosophically close to that proposed in Bassani (2001), where, however, computations are restricted to small deformations and the plastic spin is neglected.

Finally, it is noted that, in contrast with the higher-order SGP theories adopting a non-incremental treatment of dissipative strain gradients, which have been developed in the literature since the pioneering contribution of Gudmundson (2004), in the SGP model proposed in this work the onset of yielding is size-independent. However, the employed smooth elastic–plastic transition model leads to the prediction of some strengthening (that is, an increase of the *apparent* yield stress with diminishing size) since the rate of plasticity vanishes at the onset of yielding. This allows the size-dependent hardening to begin to influence the response before plasticity is observable in the stress–strain curve (Rubin and Bardella, 2023). It is believed that this is physically more reliable than the prediction of strengthening precisely at the onset of yielding, when plasticity is still absent, that has been ascribed to complicated mathematics (Chiricotto et al., 2016) within the context of non-incremental SGP theories, which also feature other drawbacks (Fleck et al., 2014; Bardella and Panteghini, 2015).

5.4.2. Directional hardening coupled with the (size-dependent) isotropic hardening

Motivated by the work in Bodner (1985) and Chan et al. (1988) the Bauschinger effect is modeled by introducing a symmetric directional hardening matrix β_{ij}, a unit matrix U_{ij}, and a scalar measure β of directional hardening by the equations

$$\dot{\beta}_{ij} = m_\beta \Gamma (\beta_s U_{ij} - \beta_{ij})\,, \quad \mathbf{U} = \frac{\mathbf{B}''_e}{|\mathbf{B}''_e|}\,, \quad U_{ij} = \mathbf{U}\cdot(\mathbf{m}'_i \otimes \mathbf{m}'_j)\,, \quad U^{ij} = \mathbf{U}\cdot(\mathbf{m}^{i\prime}\otimes\mathbf{m}^{j\prime})\,, \quad \beta = \boldsymbol{\beta}\cdot\mathbf{U} = \beta_{ij}U^{ij}\,, \tag{36}$$

such that $\boldsymbol{\beta} = \beta_{ij}\mathbf{m}^{i\prime}\otimes\mathbf{m}^{j\prime}$ and $\beta_{ij} = \boldsymbol{\beta}\cdot(\mathbf{m}'_i\otimes\mathbf{m}'_j)$. Here, the material parameter $m_\beta \geq 0$ controls the rate at which β_{ij} approaches the matrix $\beta_s U_{ij}$. Since $\mathbf{U}$ has unit modulus, it follows that for monotonic proportional loading β approaches its saturated value β_s.

Then, the Bauschinger effect is modeled by specifying the yield value y in (32) in the form

$$y = Y(1+\beta)\,. \tag{37}$$

For proportional loading, U_{ij} is constant during loading and it changes sign during reverse loading. Since β_{ij} is constant during elastic response with $\Gamma = 0$, the value of β changes sign during reverse loading when $\mathbf{B}''_e = \mathbf{0}$ and the effective yield value changes from $y = Y(1+|\beta|)$ to $y = Y(1-|\beta|)$, which reduces the effective yield value during reverse loading, modeling the Bauschinger effect. Moreover, to ensure that y remains positive, β_s is limited to the range $\beta_s \in [0,1)$.

6. Application: finite cyclic torsion of thin metal wires

The torsion of polycrystalline metal wires in the size range spanning from tens of nanometers to tens of micrometers is a benchmark that has been extensively used in the literature both to investigate size-effects experimentally, since the pivotal contribution (Fleck et al., 1994) to most recent efforts exploring cyclic loading (Liu et al., 2013), and to unveil the capabilities of SGP theories, by considering lower-order theories (Bassani, 2001; Hwang et al., 2003) and higher-order ones (see, e.g., Panteghini and Bardella, 2020, and references therein). Within the context of lower-order SGP theories applied to the homogenized wire where lattice and grain details are neglected, as considered here, the torsion benchmark has the advantage that it does not need higher-order boundary conditions to trigger gradients of plastic flow. Moreover, lower-order SGP applied to torsion allows plasticity to freely develop at the external surface, that is consistent with the most common situation in which dislocations can exit the wire when they reach its boundary. This may not be the case if the wire surface is passivated.

6.1. Kinematics

Consider an elastically isotropic solid circular cylinder with constant outer radius a experiencing cyclic torsional loading. The cylindrical polar base vectors $(\mathbf{e}_r, \mathbf{e}_\theta, \mathbf{e}_z)$ are defined relative to the fixed orthonormal triad of vectors $\mathbf{e}_i$ by the expressions

$$\mathbf{e}_r = \cos(\hat{\theta})\mathbf{e}_1 + \sin(\hat{\theta})\mathbf{e}_2\,, \quad \mathbf{e}_\theta = -\sin(\hat{\theta})\mathbf{e}_1 + \cos(\hat{\theta})\mathbf{e}_2\,, \quad \mathbf{e}_z = \mathbf{e}_3\,, \quad \hat{\theta} = \theta + \kappa z\,,$$

where $\kappa(t)$ is the torsional twist. Also, the current location $\mathbf{x}$ of a material point is given by

$$\mathbf{x} = r\mathbf{e}_r(\hat{\theta}) + z\mathbf{e}_z\,, \quad \theta^1 = r\,, \quad \theta^2 = \theta(\hat{\theta})\,, \quad \theta^3 = z\,, \tag{38}$$

where θ^i are convected coordinates. Note that the kinematics in Eq. (38) assumes the absence of motion along the radial coordinate.[1] Since the main objective of this example is to examine the Eulerian rates of elastic incompatibilities R_{ij} in (11), it is assumed that a body force, which will be more precisely specified later, is applied to satisfy the equilibrium equation. It then follows that the covariant base vectors $\mathbf{g}_i$ and the contravariant base vectors $\mathbf{g}^i$ are specified by

$$\begin{aligned}&\mathbf{g}_1 = \mathbf{x}_{,1} = \mathbf{e}_r\,, \quad \mathbf{g}_2 = \mathbf{x}_{,2} = r\mathbf{e}_\theta\,, \quad \mathbf{g}_3 = \mathbf{x}_{,3} = r\kappa\mathbf{e}_\theta + \mathbf{e}_z\,, \quad g^{1/2} = \mathbf{g}_1\times\mathbf{g}_2\cdot\mathbf{g}_3 = r\,,\\ &\mathbf{g}^1 = g^{-1/2}\mathbf{g}_2\times\mathbf{g}_3 = \mathbf{e}_r\,, \quad \mathbf{g}^2 = g^{-1/2}\mathbf{g}_3\times\mathbf{g}_1 = \frac{1}{r}\mathbf{e}_\theta - \kappa\mathbf{e}_z\,, \quad \mathbf{g}^3 = g^{-1/2}\mathbf{g}_1\times\mathbf{g}_2 = \mathbf{e}_z\,.\end{aligned} \tag{39}$$

Moreover, the associated velocity $\mathbf{v}$, velocity gradient $\mathbf{L}$, and equivalent distortional deformation rate $\dot\varepsilon$ are given by

$$\begin{aligned}&\mathbf{v} = \dot{\mathbf{x}} = rz\dot\kappa\mathbf{e}_\theta\,,\\ &\mathbf{L} = \dot{\mathbf{g}}_i\otimes\mathbf{g}^i = z\dot\kappa\mathbf{e}_\theta\otimes\mathbf{e}_r - rz\dot\kappa\mathbf{e}_r\otimes\Big(\frac{1}{r}\mathbf{e}_\theta - \kappa\mathbf{e}_z\Big) + \big(r\dot\kappa\mathbf{e}_\theta - rz\kappa\dot\kappa\mathbf{e}_r\big)\otimes\mathbf{e}_z\\ &\quad = z\dot\kappa(-\mathbf{e}_r\otimes\mathbf{e}_\theta + \mathbf{e}_\theta\otimes\mathbf{e}_r) + r\dot\kappa(\mathbf{e}_\theta\otimes\mathbf{e}_z)\,, \quad \dot\varepsilon = \frac{r|\dot\kappa|}{\sqrt{3}}\,.\end{aligned} \tag{40}$$

6.2. Purely elastic response and its compatibility

In the absence of plasticity ($\mathbf{L}_p = \mathbf{0}$) the evolution Eq. (3) is solved subject to the initial conditions

$$\mathbf{m}_1 = \mathbf{E}_r\,, \quad \mathbf{m}_2 = \mathbf{E}_\theta\,, \quad \mathbf{m}_3 = \mathbf{E}_z = \mathbf{e}_z \quad \text{for} \quad \kappa = 0\,,$$

where $\mathbf{E}_r = \mathbf{e}_r(\kappa = 0)$ and $\mathbf{E}_\theta = \mathbf{e}_\theta(\kappa = 0)$. These initial conditions can be conveniently selected because the initial state is assumed to be a zero-stress state. Then, the elastic solution of (3) is given by

$$\begin{aligned}&\mathbf{m}_1 = \mathbf{e}_r\,, \quad \mathbf{m}_2 = \mathbf{e}_\theta\,, \qquad\quad \mathbf{m}_3 = r\kappa\mathbf{e}_\theta + \mathbf{e}_z\,,\\ &\mathbf{m}^1 = \mathbf{e}_r\,, \quad \mathbf{m}^2 = \mathbf{e}_\theta - r\kappa\mathbf{e}_z\,, \quad \mathbf{m}^3 = \mathbf{e}_z\,.\end{aligned} \tag{41}$$

Also, the reciprocal vectors $\mathbf{M}^i$ are given by

$$\mathbf{M}^1 = \mathbf{E}_r\,, \quad \mathbf{M}^2 = \mathbf{E}_\theta\,, \quad \mathbf{M}^3 = \mathbf{E}_z\,,$$

so $\mathbf{F}_m$ in Eq. (7) becomes

$$\mathbf{F}_m = \mathbf{m}_1\otimes\mathbf{E}_r + \mathbf{m}_2\otimes\mathbf{E}_\theta + \mathbf{m}_3\otimes\mathbf{E}_z = \mathbf{e}_r\otimes\mathbf{E}_r + \mathbf{e}_\theta\otimes\mathbf{E}_\theta + \big(r\kappa\mathbf{e}_\theta + \mathbf{e}_z\big)\otimes\mathbf{E}_z\,, \quad \dot{\mathbf{F}}_m = \mathbf{L}\mathbf{F}_m\,, \quad \mathbf{F}_m(\kappa = 0) = \mathbf{I}\,.$$

Next, from Eq. (39) it follows that

$$\mathbf{G}^1 = \mathbf{E}_r\,, \quad \mathbf{G}^2 = \frac{1}{r}\mathbf{E}_\theta\,, \quad \mathbf{G}^3 = \mathbf{E}_z\,, \tag{42}$$

so that, with the help of Eqs. (38) and (43), one has

$$\mathrm{Curl}(\mathbf{F}_m) = -\frac{\mathbf{F}_m}{\partial r}\times\mathbf{E}_r - \frac{\mathbf{F}_m}{\partial\theta}\times\frac{1}{r}\mathbf{E}_\theta - \frac{\mathbf{F}_m}{\partial z}\times\mathbf{E}_z\,. \tag{43}$$

In addition,

$$\begin{aligned}&\frac{\partial\mathbf{F}_m}{\partial r} = \kappa\mathbf{e}_\theta\otimes\mathbf{E}_z\,,\\ &\frac{\partial\mathbf{F}_m}{\partial\theta} = \mathbf{e}_\theta\otimes\mathbf{E}_r + \mathbf{e}_r\otimes\mathbf{E}_\theta - \mathbf{e}_r\otimes\mathbf{E}_\theta - \mathbf{e}_\theta\otimes\mathbf{E}_r - r\kappa\mathbf{e}_r\otimes\mathbf{E}_z\,,\\ &\frac{\partial\mathbf{F}_m}{\partial z} = \kappa\mathbf{e}_\theta\otimes\mathbf{E}_r - \kappa\mathbf{e}_r\otimes\mathbf{E}_\theta - r\kappa^2\mathbf{e}_r\otimes\mathbf{E}_z\,,\end{aligned}$$

so that

$$\mathrm{Curl}(\mathbf{F}_m) = -\kappa\mathbf{e}_\theta\otimes\mathbf{E}_\theta - \frac{1}{r}\big(\mathbf{e}_\theta\otimes\mathbf{E}_z - \mathbf{e}_\theta\otimes\mathbf{E}_z + r\kappa\mathbf{e}_r\otimes\mathbf{E}_r\big) - \big(-\kappa\mathbf{e}_\theta\otimes\mathbf{E}_\theta - \kappa\mathbf{e}_r\otimes\mathbf{E}_r\big) = \mathbf{0}\,.$$

6.3. Elastoplastic response

Since $\mathbf{L}$ and $\mathbf{L}_p$ are deviatoric tensors, $\mathbf{m}_i' = \mathbf{m}_i$ and $J_e = 1$, and it can be shown that for this torsion problem

$$\begin{aligned}&\mathbf{m}_1 = m_{1r}\mathbf{e}_r\,, && \mathbf{m}_2 = m_{2\theta}\mathbf{e}_\theta + m_{2z}\mathbf{e}_z\,, && \mathbf{m}_3 = m_{3\theta}\mathbf{e}_\theta + m_{3z}\mathbf{e}_z\,,\\ &\mathbf{m}^1 = (m_{2\theta}m_{3z} - m_{2z}m_{3\theta})\mathbf{e}_r\,, && \mathbf{m}^2 = m_{1r}m_{3z}\mathbf{e}_\theta - m_{1r}m_{3\theta}\mathbf{e}_z\,, && \mathbf{m}^3 = -m_{1r}m_{2z}\mathbf{e}_\theta + m_{1r}m_{2\theta}\mathbf{e}_z\,,\\ &J_e = m_{1r}(m_{2\theta}m_{3z} - m_{2z}m_{3\theta}) = 1\,.\end{aligned} \tag{44}$$

[1] Hwang et al. (2003) deal with finite torsion, within a lower-order mechanism-based SGP (Huang et al., 2000), by allowing for richer kinematics, including motion along the radial direction. However, Hwang et al. (2003) consider a Lagrangian finite-deformation framework and neglect distinction between elasticity and plasticity in a deformation theory of plasticity, modeling monotonic proportional loading only.

with $\mathbf{B}'_e$ and $\mathbf{B}'^{-1}_e$ expressed in the forms (25). Therefore, with the help of Eq. (25), the matrix of components of $\mathbf{B}'_e$ with respect to the base $(\mathbf{e}_r, \mathbf{e}_\theta, \mathbf{e}_z)$ become

$$\mathbf{B}'_e = \begin{bmatrix} m_{1r}^2 & 0 & 0 \\ 0 & m_{2\theta}^2 + m_{3\theta}^2 & m_{2\theta}m_{2z} + m_{3\theta}m_{3z} \\ 0 & m_{2\theta}m_{2z} + m_{3\theta}m_{3z} & m_{2z}^2 + m_{3z}^2 \end{bmatrix} \tag{45}$$

This form of $\mathbf{B}'_e$ indicates that $T_{r\theta} = T_{rz} = 0$. Moreover, since the stress components are independent of θ and z, the components b_r, b_θ, b_z of the body force per unit mass needed to satisfy equilibrium can be determined by

$$\rho_r b_r = -\big(\frac{\partial T_{rr}}{\partial r} + \frac{T_{rr} - T_{\theta\theta}}{r}\big)\,, \quad b_\theta = b_z = 0\,.$$

Alternatively, the material can be modeled as incompressible and the pressure can be determined by solving this equation with $b_r = 0$.

In addition, since

$$\mathbf{m}_1 \cdot \mathbf{m}_2 = \mathbf{m}_1 \cdot \mathbf{m}_3 = 0\,, \quad \mathbf{m}_2 \cdot \mathbf{m}_3 = m_{2\theta}m_{3\theta} + m_{2z}m_{3z}\,,$$

it follows from (27) that the plastic spins Ω_{12}, Ω_{31} vanish and

$$\Gamma = \frac{b_1}{\sqrt{3}}|\dot\kappa|\, r\langle g\rangle\,, \quad \Omega_{23} = \frac{b_1}{2\sqrt{3}}|\dot\kappa|\, r\langle g\rangle \bar\Omega_{23}\chi_{23}(m_{2\theta}m_{3\theta} + m_{2z}m_{3z})\,, \quad \chi_{23} = \frac{2}{\pi}\tan^{-1}\Big[\frac{m_{3\theta}^2 + m_{3z}^2 - m_{2\theta}^2 - m_{2z}^2}{2(m_{2\theta}m_{3\theta} + m_{2z}m_{3z})}\Big]. \tag{46}$$

Moreover, for this case (27) can be rewritten as

$$\mathbf{L}_p = \frac{\Gamma}{2}\big[\mathbf{I} - \frac{3\mathbf{B}'^{-1}_e}{\mathrm{tr}(\mathbf{B}'^{-1}_e)} + \bar\Omega_{23}\chi_{23}\mathbf{m}_2 \cdot \mathbf{m}_3(\mathbf{m}^2 \otimes \mathbf{m}^2 - \mathbf{m}^3 \otimes \mathbf{m}^3)\big]\,,$$

where

$$\mathrm{tr}(\mathbf{B}'^{-1}_e) = m_{1r}^{-2} + m_{1r}^2(m_{2\theta}^2 + m_{2z}^2 + m_{3\theta}^2 + m_{3z}^2) \tag{47}$$

and

$$\mathbf{m}^2 \otimes \mathbf{m}^2 - \mathbf{m}^3 \otimes \mathbf{m}^3 = m_{1r}^2(\mathbf{e}_\theta \otimes \mathbf{e}_z - \mathbf{e}_z \otimes \mathbf{e}_\theta)\,.$$

Therefore, the non-vanishing components of $\mathbf{L}_p$ relative to the cylindrical polar base vectors are given by

$$\begin{aligned}
L_{prr} &= \frac{\Gamma}{2}\big(1 - \frac{3}{\mathrm{tr}(\mathbf{B}'^{-1}_e)}m_{1r}^{-2}\big)\,,\\
L_{p\theta\theta} &= \frac{\Gamma}{2}\big[1 - \frac{3}{\mathrm{tr}(\mathbf{B}'^{-1}_e)}m_{1r}^2(m_{2z}^2 + m_{3z}^2)\big]\,,\\
L_{pzz} &= \frac{\Gamma}{2}\big[1 - \frac{3}{\mathrm{tr}(\mathbf{B}'^{-1}_e)}m_{1r}^2(m_{2\theta}^2 + m_{3\theta}^2)\big]\,,\\
L_{p\theta z} &= \frac{\Gamma}{2}m_{1r}^2\big[\frac{3}{\mathrm{tr}(\mathbf{B}'^{-1}_e)}(m_{2\theta}m_{2z} + m_{3\theta}m_{3z}) + \bar\Omega_{23}\chi_{23}(m_{2\theta}m_{3\theta} + m_{2z}m_{3z})\big]\,,\\
L_{pz\theta} &= \frac{\Gamma}{2}m_{1r}^2\big[\frac{3}{\mathrm{tr}(\mathbf{B}'^{-1}_e)}(m_{2\theta}m_{2z} + m_{3\theta}m_{3z}) - \bar\Omega_{23}\chi_{23}(m_{2\theta}m_{3\theta} + m_{2z}m_{3z})\big]\,.
\end{aligned} \tag{48}$$

Furthermore,

$$\dot{\mathbf{m}}_i = \dot\kappa\Big[\big(\frac{\partial m_{ir}}{\partial\kappa} - z m_{i\theta}\big)\mathbf{e}_r + \big(\frac{\partial m_{i\theta}}{\partial\kappa} + z m_{ir}\big)\mathbf{e}_\theta + \frac{\partial m_{iz}}{\partial\kappa}\mathbf{e}_z\Big]\,, \tag{49}$$

so the non-trivial evolution Eqs. (29) require

$$\begin{aligned}
\frac{\partial m_{1r}}{\partial\kappa} &= -r\frac{\dot\kappa}{|\dot\kappa|}\frac{b_1}{2\sqrt{3}}\langle g\rangle\big(m_{1r} - \frac{3}{m_{1r}\mathrm{tr}(\mathbf{B}'^{-1}_e)}\big)\,,\\
\frac{\partial m_{2\theta}}{\partial\kappa} &= r\Big\{\, m_{2z} - \frac{\dot\kappa}{|\dot\kappa|}\frac{b_1}{2\sqrt{3}}\langle g\rangle\Big[\, m_{2\theta} - \frac{3m_{1r}m_{3z}}{\mathrm{tr}(\mathbf{B}'^{-1}_e)} + \bar\Omega_{23}\chi_{23}(m_{2\theta}m_{3\theta} + m_{2z}m_{3z})m_{1r}m_{2z}\,\Big]\Big\}\,,\\
\frac{\partial m_{2z}}{\partial\kappa} &= -r\frac{\dot\kappa}{|\dot\kappa|}\frac{b_1}{2\sqrt{3}}\langle g\rangle\Big[\, m_{2z} + \frac{3m_{1r}m_{3\theta}}{\mathrm{tr}(\mathbf{B}'^{-1}_e)} - \bar\Omega_{23}\chi_{23}(m_{2\theta}m_{3\theta} + m_{2z}m_{3z})m_{1r}m_{2\theta}\,\Big]\,,\\
\frac{\partial m_{3\theta}}{\partial\kappa} &= r\Big\{\, m_{3z} - \frac{\dot\kappa}{|\dot\kappa|}\frac{b_1}{2\sqrt{3}}\langle g\rangle\Big[\, m_{3\theta} + \frac{3m_{1r}m_{2z}}{\mathrm{tr}(\mathbf{B}'^{-1}_e)} + \bar\Omega_{23}\chi_{23}(m_{2\theta}m_{3\theta} + m_{2z}m_{3z})m_{1r}m_{3z}\,\Big]\Big\}\,,\\
\frac{\partial m_{3z}}{\partial\kappa} &= -r\frac{\dot\kappa}{|\dot\kappa|}\frac{b_1}{2\sqrt{3}}\langle g\rangle\Big[\, m_{3z} - \frac{3m_{1r}m_{2\theta}}{\mathrm{tr}(\mathbf{B}'^{-1}_e)} - \bar\Omega_{23}\chi_{23}(m_{2\theta}m_{3\theta} + m_{2z}m_{3z})m_{1r}m_{3\theta}\,\Big]\,,
\end{aligned} \tag{50}$$

which are consistent with $J_e = 1$ in Eq. (44). These equations are integrated subject to the initial conditions

$$\kappa(0) = 0\,, \quad m_{1r}(r,0) = 1\,, \quad m_{2\theta}(r,0) = 1\,, \quad m_{2z}(r,0) = 0\,, \quad m_{3\theta}(r,0) = 0\,, \quad m_{3z}(r,0) = 1\,. \tag{51}$$

For small elastic deformations the triad $\mathbf{m}'_i$ remains nearly orthonormal. Consequently, to examine the counterclockwise rotation of $\mathbf{m}'_2$ and $\mathbf{m}'_3$ about the axis $\mathbf{m}'_1$, it is convenient to define the average angle θ_{23}, such that

$$\theta_{23} = \frac{1}{2}\left[\tan^{-1}\left(\frac{m_{2z}}{m_{2\theta}}\right) - \tan^{-1}\left(\frac{m_{3\theta}}{m_{3z}}\right)\right]. \tag{52}$$

It follows from Eq. (50) that for monotonic loading with $\dot{\kappa} > 0$ the initial elastic response causes θ_{23} to decrease, which represents a clockwise rotation of the triad $\mathbf{m}'_i$ about the $\mathbf{m}'_1$ axis. The influence of $\bar{\Omega}_{23}$ on the rotation of the triad will be discussed later with reference to Fig. 7.

For later reference, it is convenient to also define the difference of the counterclockwise rotations of $\mathbf{m}'_2$ and $\mathbf{m}'_3$ about the axis $\mathbf{m}'_1$

$$\Delta\theta_{23} = \tan^{-1}\left(\frac{m_{2z}}{m_{2\theta}}\right) + \tan^{-1}\left(\frac{m_{3\theta}}{m_{3z}}\right). \tag{53}$$

To evaluate the elastic incompatibility measures in Eq. (11) it can be shown that

$$\begin{aligned}
&\mathbf{L}_p = L_{prr}\mathbf{e}_r\otimes\mathbf{e}_r + L_{p\theta\theta}(\mathbf{e}_\theta\otimes\mathbf{e}_\theta) + L_{p\theta z}(\mathbf{e}_\theta\otimes\mathbf{e}_z) + L_{pz\theta}(\mathbf{e}_z\otimes\mathbf{e}_\theta) + L_{pzz}(\mathbf{e}_z\otimes\mathbf{e}_z),\\
&\operatorname{curl}(\mathbf{L}_p) = -\frac{\partial\mathbf{L}_p}{\partial r}\times\mathbf{e}_r - \frac{\partial\mathbf{L}_p}{\partial\theta}\times\left(\frac{1}{r}\mathbf{e}_\theta - \kappa\mathbf{e}_z\right) - \frac{\partial\mathbf{L}_p}{\partial z}\times\mathbf{e}_z,
\end{aligned} \tag{54}$$

where the components are functions of (r,κ). It then follows that

$$\begin{aligned}
\operatorname{curl}(\mathbf{L}_p) = &-\frac{L_{p\theta z}}{r}(\mathbf{e}_r\otimes\mathbf{e}_r) - \frac{\partial L_{p\theta z}}{\partial r}(\mathbf{e}_\theta\otimes\mathbf{e}_\theta) + \left(\frac{\partial L_{p\theta\theta}}{\partial r} + \frac{L_{p\theta\theta} - L_{prr}}{r}\right)(\mathbf{e}_\theta\otimes\mathbf{e}_z)\\
&- \frac{\partial L_{pzz}}{\partial r}(\mathbf{e}_z\otimes\mathbf{e}_\theta) + \left(\frac{\partial L_{pz\theta}}{\partial r} + \frac{L_{pz\theta}}{r}\right)(\mathbf{e}_z\otimes\mathbf{e}_z),
\end{aligned} \tag{55}$$

where the diagonal terms, due to $L_{p\theta z}$ and $L_{pz\theta}$, are the sole non-vanishing contributions to $\operatorname{curl}(\mathbf{L}_p)$ under small strains and rotations (Bardella and Panteghini, 2015). Since the deformation is isochoric with $J_e = 1$, the stress $\mathbf{T}$ in (31) is deviatoric. Also, using Eqs. (11), (44), and (55) it can be shown that the non-vanishing components of R_{ij} are

$$\begin{aligned}
R_{11} &= \frac{L_{p\theta z}}{r}m_{1r}^2,\\
R_{22} &= \frac{\partial L_{p\theta z}}{\partial r}m_{2\theta}^2 - \left(\frac{\partial L_{p\theta\theta}}{\partial r} + \frac{L_{p\theta\theta} - L_{prr}}{r}\right)m_{2\theta}m_{2z} + \frac{\partial L_{pzz}}{\partial r}m_{2\theta}m_{2z} - \left(\frac{\partial L_{pz\theta}}{\partial r} + \frac{L_{pz\theta}}{r}\right)m_{2z}^2,\\
R_{33} &= \frac{\partial L_{p\theta z}}{\partial r}m_{3\theta}^2 - \left(\frac{\partial L_{p\theta\theta}}{\partial r} + \frac{L_{p\theta\theta} - L_{prr}}{r}\right)m_{3\theta}m_{3z} + \frac{\partial L_{pzz}}{\partial r}m_{3\theta}m_{3z} - \left(\frac{\partial L_{pz\theta}}{\partial r} + \frac{L_{pz\theta}}{r}\right)m_{3z}^2,\\
R_{23} &= \frac{\partial L_{p\theta z}}{\partial r}m_{2\theta}m_{3\theta} - \left(\frac{\partial L_{p\theta\theta}}{\partial r} + \frac{L_{p\theta\theta} - L_{prr}}{r}\right)m_{2\theta}m_{3z} + \frac{\partial L_{pzz}}{\partial r}m_{2z}m_{3\theta} - \left(\frac{\partial L_{pz\theta}}{\partial r} + \frac{L_{pz\theta}}{r}\right)m_{2z}m_{3z},\\
R_{32} &= \frac{\partial L_{p\theta z}}{\partial r}m_{2\theta}m_{3\theta} - \left(\frac{\partial L_{p\theta\theta}}{\partial r} + \frac{L_{p\theta\theta} - L_{prr}}{r}\right)m_{2z}m_{3\theta} + \frac{\partial L_{pzz}}{\partial r}m_{2\theta}m_{3z} - \left(\frac{\partial L_{pz\theta}}{\partial r} + \frac{L_{pz\theta}}{r}\right)m_{2z}m_{3z}.
\end{aligned} \tag{56}$$

To better understand the influence of the plastic spin, it is noted from Eq. (56) that

$$\sum_{i=1}^{3}\sum_{i=j}^{3} R_{ij} = \frac{L_{p\theta z}}{r}m_{1r}^2 + \frac{\partial L_{p\theta z}}{\partial r}(m_{2\theta} + m_{3\theta})^2 - \left(\frac{\partial L_{pz\theta}}{\partial r} + \frac{L_{pz\theta}}{r}\right)(m_{2z} + m_{3z})^2 + f(L_{prr}, L_{p\theta\theta}, L_{pzz}),$$

where, for the purpose of this discussion, there is no need to explicitly record the lengthy function $f(L_{prr}, L_{p\theta\theta}, L_{pzz})$. Next, using the approximation of small strains and rotations, this expression for the torsion problem reduces to

$$\sum_{i=1}^{3}\sum_{i=j}^{3} R_{ij} = \frac{L_{p\theta z} - L_{pz\theta}}{r} + \frac{\partial(L_{p\theta z} - L_{pz\theta})}{\partial r} = 2\left(\frac{W_{p\theta z}}{r} + \frac{\partial W_{p\theta z}}{\partial r}\right), \tag{57}$$

which depends on the plastic spin rate only, in agreement with (Bardella and Panteghini, 2015). It is remarked that, for clarity, the full finite-deformation equations will be solved in all the following simulations.

6.4. Results and discussion

The size-effect in torsion can be displayed by plotting the normalized torque Q/a^3 as a function of the non-dimensional twist κa, also representing the outer surface shear strain, where

$$Q = 2\pi\mu\int_0^a B_{e\theta z}r^2\mathrm{d}r. \tag{58}$$

6.4.1. Numerical solution

The torsion problem has been solved with the commercial software Mathematica® using the `NDSolve` function, where the values of the time-integration parameters `AccuracyGoal` and `PrecisionGoal` are specified to be equal and are here denoted as `NDSGoal`. In most of the following simulations, `NDSGoal` has been set equal to 13, although `NDSGoal=10` is enough to obtain adequate accuracy for several fields of interest in most analyses.

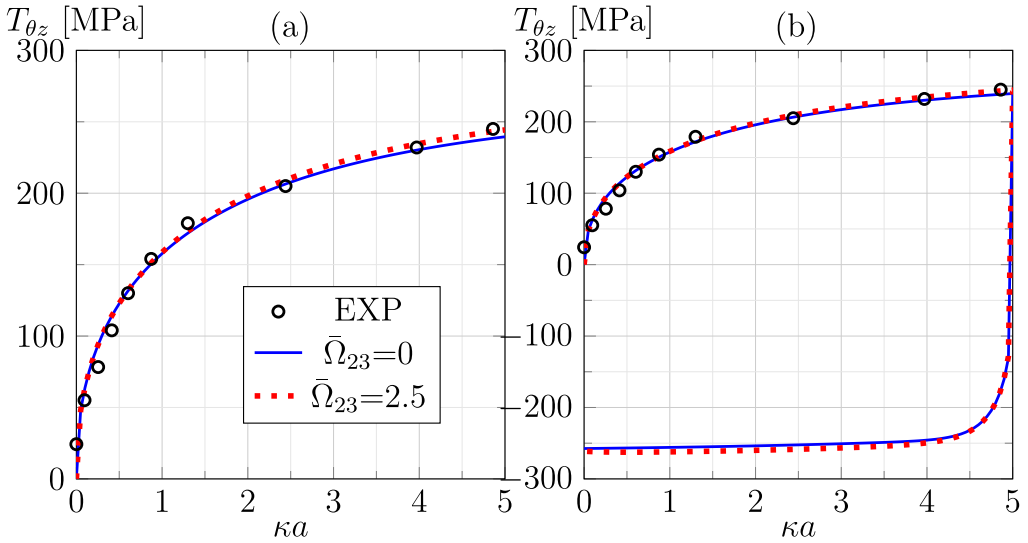

Fig. 1. Large-deformation torsion of oxygen free electronic grade (OFE) copper at room temperature: comparison, in terms of the surface shear stress $T_{\theta z}(r=a)$, (a) between experimental data of Stout and Rollett (1990) (hollow black circles), taken from (Bodner and Rubin, 1994), and simulations of size-independent plasticity ($\ell=0$). Figure (b) includes simulations of cyclic loading.

The numerical integration has been performed by integrating over both κ and r in order to conveniently obtain the required derivatives with respect to r. Therefore, `NDSolve` has been employed as a solver for partial differential equations. Moreover, to solve the problem for cyclic loading, the applied twist has been specified as a function of time t, $\kappa(t)$. Different functions $\kappa(t)$, such as piecewise linear and sinusoidal, have been tested to check the solution accuracy. In the absence of size-dependent hardening, the problem could be solved, also under cyclic loading, by integrating directly in κ, i.e. without introducing time, and even by adopting, instead of `NDSolve`, the function `ParametricNDSolve`, which allows for the solution of a system of ordinary differential equations by introducing r as a parameter. The consistency of the results obtained from all these tests ensure their accuracy. However, because of the high nonlinearity of the problem, in some analyses, the field ξ turns out to be affected by some inaccuracies in an annular region near the outer boundary. These inaccuracies seem to be non-monotonic for changes in the material parameters entering the evolution equation for ξ, especially for thin wires. They typically show up after the second loading reversal and, then, they may even cause unphysical solutions. To avoid such inaccuracies, the boundary value problem has been solved for fictitious larger wires, typically of radius $\tilde{a}=1.3a$, while the results and, in particular, the computation of the torque (58), have been limited to the region $r\in[0,a]$. By trying different combinations of domain size $\tilde{a}$, material parameters, and integration parameters, this procedure has been tested to provide reliable results.

6.4.2. *Size-independent plasticity*

Size-independent plasticity including both isotropic and directional hardening can be obtained by specifying ℓ=0. Unless otherwise stated, for all simulations, the size-independent material constants, obtained by fitting the experimental data of Stout and Rollett (1990), as illustrated in Fig. 1, are specified by

$$\mu=44\,\text{GPa}\,,\quad b_1=3000\,,\quad m_H=1.8\times10^{-3}\,,\quad Y_{H0}=10^{-5}\,,\quad Y_{Hs}=3\times10^{-3}\,,\quad m_\beta=0.02\,,\quad \beta_s=0.6\,,\quad \bar{\Omega}_{23}=2.5\,.$$

Note that this torsion problem is independent of the bulk modulus k introduced in Eq. (30). Fig. 1 also shows the behavior predicted under cyclic loading due to the selected hardening parameters and the negligible effect of the plastic spin rate on the stress response for size-independent plasticity (ℓ=0).

6.4.3. *Size-dependent plasticity*

Unless otherwise stated, the material constants m_ℓ, m_r, Y_{Rs}, n_R controlling the size-dependence are specified by

$$m_\ell=15.\,,\quad m_r=1.\,,\quad Y_{Rs}=3\times10^{-3}\,,\quad n_R=0.3\,. \tag{59}$$

The material length scale ℓ will be varied within $a/\ell\in[1,\infty)$ to illustrate the predicted size-effect, although, when focusing on the features of the fields related to the inclusion of plastic rate gradients in the modeling, only the "strongest wire" $a/\ell=1$ will be considered.

The small ratio m_r/m_ℓ in Eq. (59) indicates that the rate of recovery of hardening in (34) is set to be much smaller than the rate of increase of hardening. This may be consistent with the behavior of densities of GNDs that, after piling up at grain boundaries under monotonic loading, may find it more difficult to annihilate because of the contextual development of forest dislocations, or other substructures of dislocations.

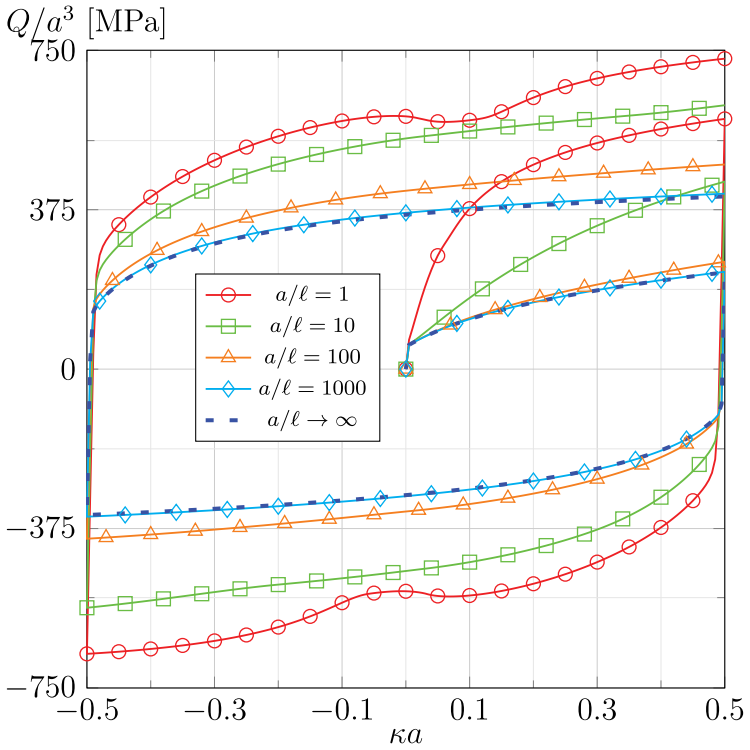

Fig. 2. Normalized torque vs non-dimensional twist: Comparison of the predictions at different wire radii under cyclic loading.

Fig. 2 shows the predictions for the normalized torque as a function of the non-dimensional twist κa, at variable wire radii. The main result shown in this figure is that the proposed model can predict a significant size-dependent hardening effect with increase in strength for reduction in the wire radius. The parameter $n_R = 0.3$ has been selected so that the behavior for $a/\ell = 10^3$ is very close to size-independent plasticity (i.e., $a/\ell \to \infty$). Given both the purposes of this investigation and the lack of experimental data for the finite-deformation torsion of thin wires under cyclic loading, fitting the size-effect of real samples is left for future studies. However, it is here emphasized that the proposed model exhibits the potential to predict the known behavior of metals at sizes where densities of GNDs affect the response (Fleck et al., 1994; Greer and De Hosson, 2011; Liu et al., 2013).

Moreover, the results in Fig. 2 for the thinnest wire ($a/\ell = 1$) show a mild drop in strength, occurring near the points where reverse loading causes $\kappa a = 0$, due to annihilation of defects. These drops are due to the decrease in size-dependent hardening ensuing from the decrease of ξ, which is illustrated in Fig. 3. For the sake of clarity, some of the results are plotted as functions of the monotonically increasing loading parameter

$$\kappa_{\rm mon} = \int_0^t |\dot\kappa| \mathrm{d}t \,. \tag{60}$$

Therefore, for the cycle considered in the simulations illustrated next, in which $\kappa a \in [0, 0.5] \cup [0.5, -0.5] \cup [-0.5, 0.5]$, Eq. (60) yields $\kappa_{\rm mon} a \in [0, 2.5]$.

Fig. 3 shows the crucial dependence of ξ on $\bar\Omega_{23}$, along with the mild dependence of ξ on r. Correspondingly, as documented in Fig. 4, which focuses on $r = a$ only, Y_R is very much dependent on $\bar\Omega_{23}$ while it is almost unaffected by m_r, see Eq. (34). Instead, m_r has an enormous influence on Y_ℓ. Fig. 4 reports results for $\bar\Omega_{23} \geq 0$ only, because the sign of $\bar\Omega_{23}$ has a minimal influence on Y_R and Y_ℓ for the sets of parameters explored in this investigation, as shown later in discussing the results plotted in Fig. 6. Moreover, from Fig. 3 it is observed that when κ and $\bar\Omega_{23}$ have opposite signs ξ may decrease with increasing r, and this behavior is consistent for all the chosen sets of data. In general, the plastic spin rate introduces a directionality in the model (i.e., for a given set of material parameters, changing the sign of the loading history $\kappa(t)$ also changes the magnitude of some fields of interest); however, this effect disappears for the size-independent response ($\ell = 0$).

The dependence of the normalized torque on the rate of hardening recovery, controlled by m_r in (34), is illustrated in Fig. 5. The parameter m_r influences the drop in yield strength, occurring for small a/ℓ, near the points where reverse loading causes $\kappa a = 0$. Specifically, on the one hand, if a fast recovery is allowed ($m_r = m_\ell$) the effect of decreasing $|\xi|$ has a large influence on the torque, leading to "bumps" in the torque vs twist curve; on the other hand, hampering hardening recovery by setting $m_r = 0$ eliminates this effect. Comparison of Figs. 3, 4, and 5 clearly indicates that the drops in yield strength in Fig. 5 are due to the recovery

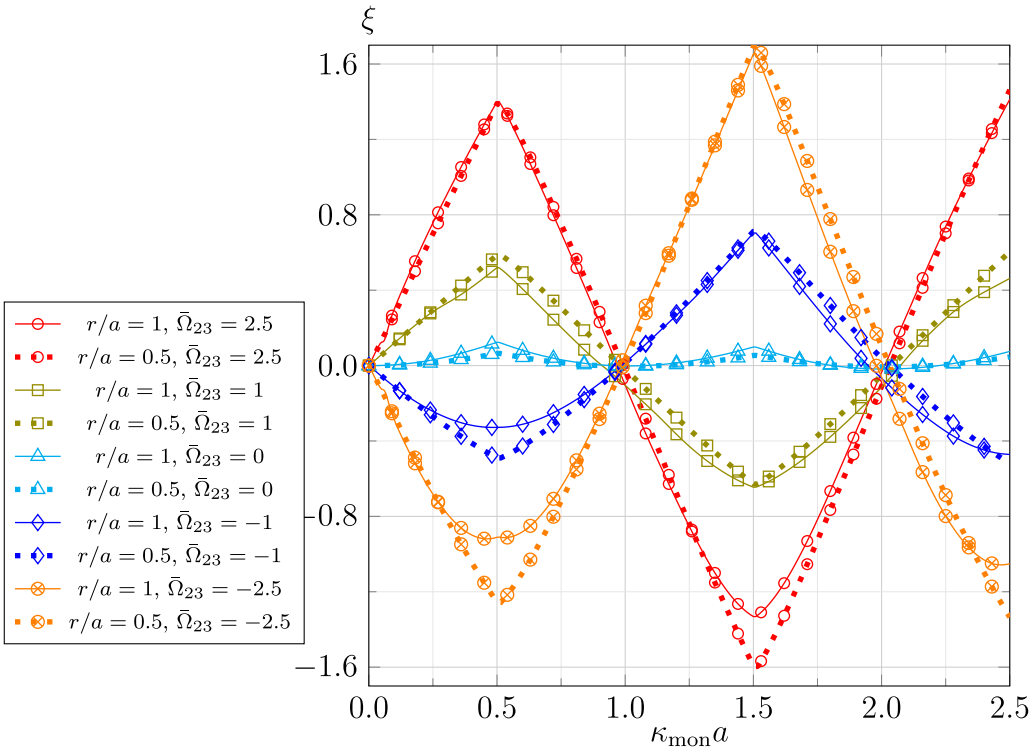

Fig. 3. ξ for different $\bar{\Omega}_{23}$ and r in terms of $\kappa_{\rm mon}$ in Eq. (60), under cyclic loading, for $a/\ell = 1$ and m_r=1 .

of the size-dependent parameter ξ. These drops in strength may cause instabilities that are not investigated here. However, it is observed that, in the literature on microscale metal plasticity, these drops, often referred to as "inflection points", are found, both experimentally and through modeling (Stoltz and Pelloux, 1976; Taillard and Pineau, 1982; Proudhon et al., 2008; Kiener et al., 2010; Wulfinghoff et al., 2015; El-Naaman et al., 2019; Reynolds and Baxter, 2000), mostly when cycling loads change sign, as in the present simulations. Also, these inflection points are associated with annihilation of GNDs via the "KIII" hardening of Asaro (1975) defined in crystal plasticity through the concept by which the last dislocation piling up in high-density GND regions is the first one to leave the pileup upon loading reversal; if this is the dominant mechanism, as in a specific regime of single-crystal plasticity under single slip, the inflection points are observed also for small deformations.

Fig. 6 shows the predictions for the normalized torque as a function of $\bar{\Omega}_{23}$. This dependence is particularly interesting because the plastic spin rate, through $\bar{\Omega}_{23}$ in this benchmark, has an enormous influence on the rates of incompatibilities, and thus on ξ. It is first noted that changing sign to $\bar{\Omega}_{23}$ has negligible influence on the torque. Second, the two curves for $a/\ell = 1$ with $\bar{\Omega}_{23} = 0$ and $a/\ell \to \infty$ are almost superposed, during the first loading branch, up to $\kappa a \approx 0.12$. On the one hand, this is consistent with the discussion about Eq. (57), indicating that in the absence of plastic spin rate the torsion response is size-independent under small strains and rotations. On the other hand, the noticeable divergence in Fig. 6 of these two curves after $\kappa a \approx 0.12$ indicates an interesting size-effect induced by finite deformations, even with zero plastic spin. Also, the curve for $\bar{\Omega}_{23} = 0$ (and $a/\ell = 1$) exhibits some mild changes of curvature due to the recovery of ξ, as seen in Fig. 3.

Finally, Fig. 7 shows the dependence of the average angle θ_{23}, as defined in Eq. (52), on the plastic spin rate through the parameter $\bar{\Omega}_{23}$. From this figure it has been numerically observed that the function θ_{23} has the symmetry

$$\theta_{23}(\kappa a, \bar{\Omega}_{23}) \ \approx \ -\theta_{23}(-\kappa a, -\bar{\Omega}_{23}),$$

with θ_{23} displaying a reversible behavior with respect to κa. Also, it is observed that the clockwise rotation of the triad is retarded when $\bar{\Omega}_{23}$ and κ have the same signs and is enhanced when they have opposite signs. It is remarked that the difference in rotation $\Delta\theta_{23}$ in (53) is related to the elastic deformations characterized by the microstructural vectors $\mathbf{m}_i$; thus, $\Delta\theta_{23}$ exhibits a behavior similar to that of the shear stress $T_{\theta z}$, the latter mirroring the behavior of the torque.

7. Concluding remarks

This investigation develops Eulerian rates of elastic incompatibilities, denoted as R_{ij}, for anisotropic elastic–inelastic materials. This Eulerian framework does not use Lagrangian tensors such as the elastic and plastic deformation tensors. Also, it relies on an

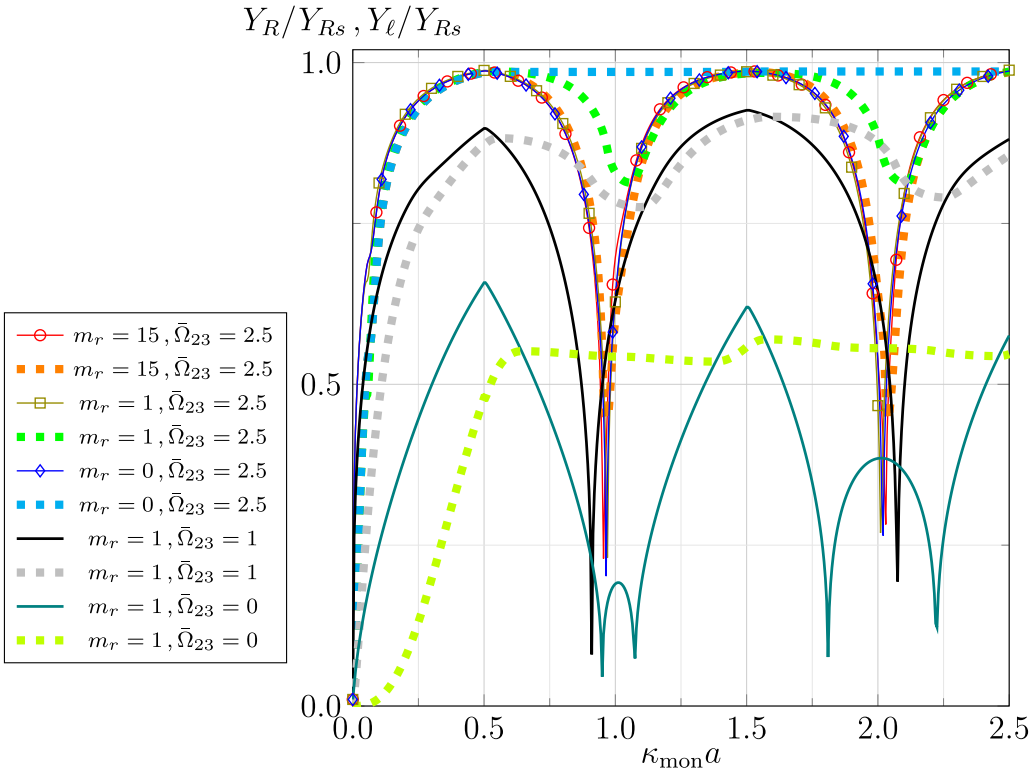

Fig. 4. Normalized Y_R (solid lines, with marks when overlapping) and Y_ℓ (thick dotted lines) for $r=a$ and different m_r and $\bar{\Omega}_{23}$ in terms of $\kappa_{\rm mon}$ in Eq. (60), under cyclic loading, for $a/\ell=1$ and $m_\ell=15$.

evolution equation, involving the rate of inelastic deformation $\mathbf{L}_p$, for the motion of three linearly independent microstructural vectors $\mathbf{m}_i$ characterizing elastic deformations and orientation changes of anisotropic directions in the material relative to a zero-stress state (Rubin, 1994).

Within this Eulerian framework, necessary and sufficient conditions for incremental incompatibilities are shown to imply that R_{ij} must be based on the curl of the inelastic rate to be evaluated in the current configuration, curl($\mathbf{L}_p$). Specifically, R_{ij} are the components of the negative of curl($\mathbf{L}_p$) relative to the distortional microstructural vectors $\mathbf{m}'_i$. As such, R_{ij} are highly nonlinear fields that for small strains and rotations particularize to the negative of the rate of the Nye-Kröner dislocation density tensor. Most importantly, each component of R_{ij} is invariant under superposed rigid body motions (SRBM) so it can be used independently in constitutive equations for material behavior. It is emphasized that, in turn, R_{ij} depend on the constitutive equation for $\mathbf{L}_p$, such that R_{ij} are not purely kinematical quantities, and, in particular, they may strongly depend on the constitutive equation for the inelastic spin rate $\mathbf{W}_p$. Also, the direct use of R_{ij} into constitutive equations seems to be quite natural within the Eulerian framework, in contrast with theories in which quantities such as curl($\mathbf{L}_p$) are included in evolution equations in the attempt to define finite kinematic quantities (see, e.g., Rubin and Bardella, 2023 for a proposal regarding a Nye-Kröner-like tensor).

As an example of the use of the foregoing features of R_{ij}, a constitutive theory for isotropically elastic materials is developed featuring a contribution to hardening that is size-dependent through a scalar field ξ defined in terms of R_{ij}, resulting in a lower-order theory of strain gradient plasticity (SGP, Bassani, 2001; Niordson and Hutchinson, 2003). To this purpose, after specializing the anisotropic theory relying on the microstructural vectors to the case of isotropic elasticity, the framework in (Rubin and Attia, 1996) is extended to account for $\mathbf{W}_p$. Then, in the spirit of modeling small-scale metal plasticity with size-dependence due to the behavior of densities of geometrically necessary dislocations (GNDs, Ashby, 1970), ξ is constructed by simply summing up all the components of R_{ij}, allowing for generation and annihilation of defects of opposite sign, and by multiplying this sum by a material length scale parameter, ℓ.

Specifically, the proposed elastoplasticity is rate-independent and characterized by a smooth elastic–inelastic transition (Hollenstein et al., 2013, 2015), where there are three contributions to hardening, all characterized by variables that saturate. The isotropic hardening consists of a conventional contribution and a size-dependent contribution, the latter allowing, through ξ, for both an increase and a decrease in hardening due to generation and annihilation, respectively, of defects. Increase and decrease of size-dependent hardening are governed by two independent parameters that permit tuning the material behavior and investigating

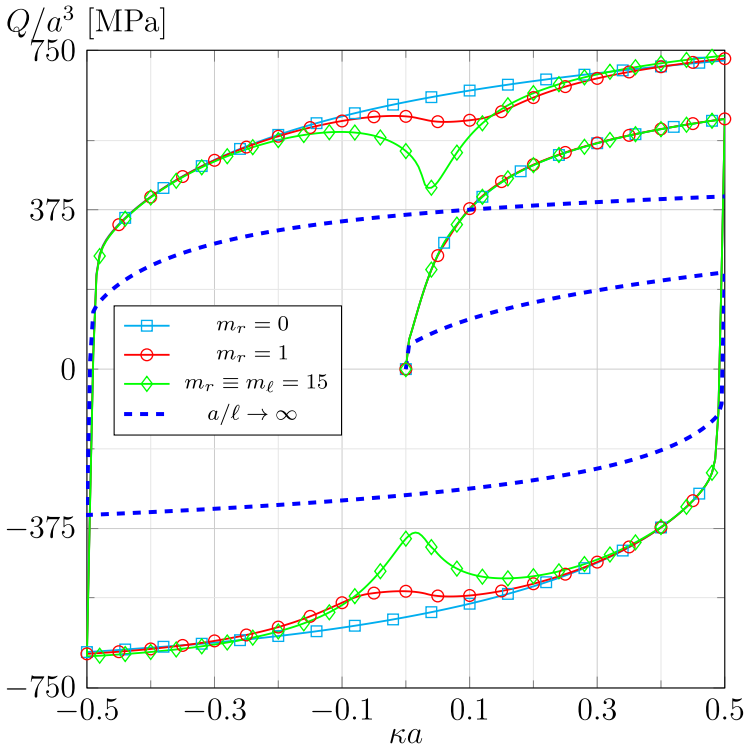

Fig. 5. Normalized torque vs non-dimensional twist: Comparison of the predictions at different m_r under cyclic loading. Unless otherwise specified, a/ℓ=1.

the influence of the field ξ on this hardening process, which depends on the loading history. The third contribution to the hardening is a directional hardening that follows Bodner (1985) and is coupled with both contributions to the isotropic hardening, thus providing the capability to model a size-dependent Bauschinger effect under complicated cyclic loading. The coupling of the smooth elastic–plastic transition with the size-dependent hardening allows for the prediction of an increase of the *apparent* yield stress with diminishing size (Rubin and Bardella, 2023).

The constitutive equation for the plastic spin $\mathbf{W}_p$ is taken from (Lee and Rubin, 2021), for its demonstrated capability of reproducing experimental data for the orientation change of the principal directions of orthotropy for uniaxial stress loading at different angles relative to the rolling direction in sheet metal forming.

The developed plasticity theory is applied to large-deformation torsion of thin metal wires subjected to cyclic loading. First, the material parameters governing the size-independent part of the model are calibrated by fitting the results of Stout and Rollett (1990) for oxygen free electronic grade copper at room temperature under monotonic torque up to an outer surface shear strain of about 5. Then, the size-dependent results of this benchmark problem demonstrate the potential of using R_{ij} directly in the constitutive equations. In particular, the obtained predictions display size-dependent results in qualitative agreement with known experimental behavior (Fleck et al., 1994; Greer and De Hosson, 2011; Liu et al., 2013), the capability of modeling generation and annihilation of densities of dislocations, and the crucial effect of the material parameter governing the plastic spin rate, in agreement with the literature on SGP (Gurtin, 2004; Bardella, 2009; Panteghini and Bardella, 2020). The torsion simulations also show the importance of the finite deformations. This is appreciated by considering that, for small strains and rotations, the adopted form of ξ depends on the plastic spin rate only, and not on the plastic strain rate, according to Bardella and Panteghini (2015). Hence, by setting the plastic spin rate to zero, it is observed that the prediction for a very thin wire (of radius equal to the material length scale ℓ) is almost identical to that for size-independent plasticity up to a surface shear strain of about 0.1, after which the size-dependent response becomes much stronger because finite-deformation effects allow the plastic strain rate to significantly influence ξ.

In future work it will be very interesting to examine the use of the proposed rates of elastic incompatibilities R_{ij} for hardening in crystal plasticity, whose basis is provided in Appendix B with the definition of $\mathbf{L}_p$ in terms of the microstructural vectors.

CRediT authorship contribution statement

M.B. Rubin: Writing – review & editing, Writing – original draft, Validation, Methodology, Investigation, Formal analysis, Conceptualization. **Lorenzo Bardella:** Writing – review & editing, Writing – original draft, Visualization, Validation, Software, Methodology, Investigation, Formal analysis, Data curation, Conceptualization.

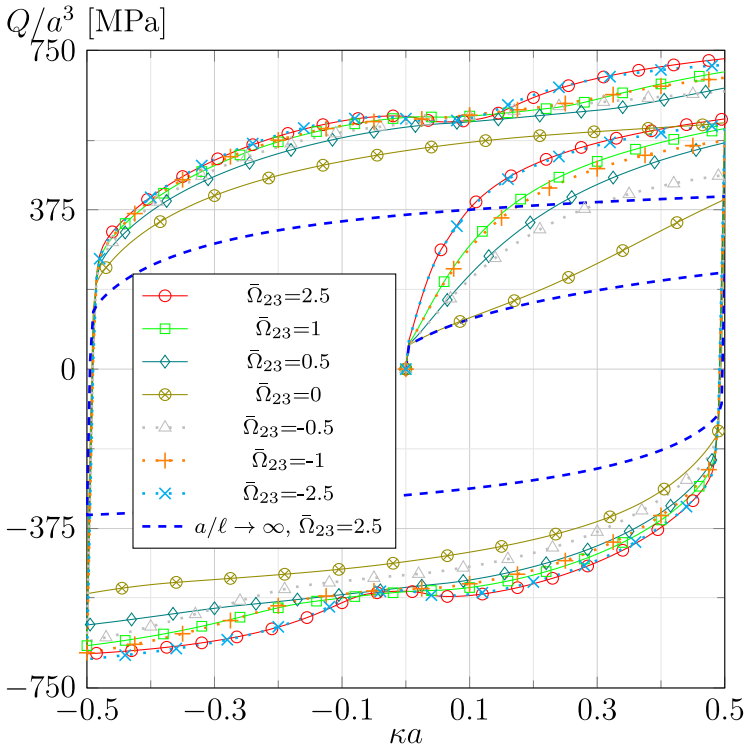

Fig. 6. Normalized torque vs non-dimensional twist: Comparison of the predictions at different $\bar{\Omega}_{23}$ under cyclic loading, for $m_r = 1$. Unless otherwise specified, $a/\ell = 1$.

Declaration of competing interest

The authors declare that they have no known competing financial interests or personal relationships that could have appeared to influence the work reported in this paper.

Acknowledgments

L.B. acknowledges the support of the Italian Ministry of Education, University, and Research (MIUR). The commercial code Mathematica® has been run at the Department of Civil, Environmental, Architectural Engineering and Mathematics of the University of Brescia, Italy, under an academic license. Also, this work was done under the auspices of GNFM (Gruppo Nazionale per la Fisica Matematica) of INDAM (Istituto Nazionale di Alta Matematica Francesco Severi).

Appendix A. Invariance under superposed rigid body motions of curl($\mathbf{L}_p$)

Under SRBM, $\mathbf{x}$ and t transform to their superposed values $\mathbf{x}^+$ and t^+ according to

$$\mathbf{x}^+ = \mathbf{c}(t) + \mathbf{Q}(t)\mathbf{x}\,, \quad t^+ = t + c\,,$$

where c is an arbitrary constant shift in time, $\mathbf{c}$ is a arbitrary vector function of time only which characterizes superposed translation, and $\mathbf{Q}$ in (18) characterizes superposed rotation. Also, $\mathbf{L}_p$ transforms to $\mathbf{L}_p^+$ and, for arbitrary convected coordinates, $(\mathbf{g}_j, \mathbf{g}^j)$ transform to $(\mathbf{g}_j^+, \mathbf{g}^{j+})$, such as

$$\mathbf{L}_p^+ = \mathbf{Q}\mathbf{L}_p\mathbf{Q}^T\,, \quad \mathbf{g}_j^+ = \mathbf{Q}\mathbf{g}_j\,, \quad \mathbf{g}^{j+} = \mathbf{Q}\mathbf{g}^j\,,$$

so that

$$\text{curl}(\mathbf{L}_p) = -\mathbf{L}_{p,j} \times \mathbf{g}^j = -(\partial \mathbf{L}_p/\partial \mathbf{x})\mathbf{g}_j \times \mathbf{g}^j\,, \quad \text{curl}^+(\mathbf{L}_p^+) = -(\partial \mathbf{L}_p^+/\partial \mathbf{x})(\partial \mathbf{x}/\partial \mathbf{x}^+)\mathbf{g}_j^+ \times \mathbf{g}^{j+} = -[\partial(\mathbf{Q}\mathbf{L}_p\mathbf{Q}^T)/\partial \mathbf{x}]\mathbf{Q}^T(\mathbf{Q}\mathbf{g}_j \times \mathbf{Q}\mathbf{g}^j)\,.$$

Next, using the results that

$$\partial(\mathbf{Q}\mathbf{L}_p\mathbf{Q}^T)/\partial \mathbf{x} = \mathbf{Q}(\partial \mathbf{L}_p/\partial \mathbf{x})\mathbf{Q}\,, \quad \mathbf{Q}\mathbf{g}_j \times \mathbf{Q}\mathbf{g}^j = \det(\mathbf{Q})\mathbf{Q}^{-T}(\mathbf{g}_j \times \mathbf{g}^j) = (\mathbf{g}_j \times \mathbf{g}^j)\mathbf{Q}^T\,,$$

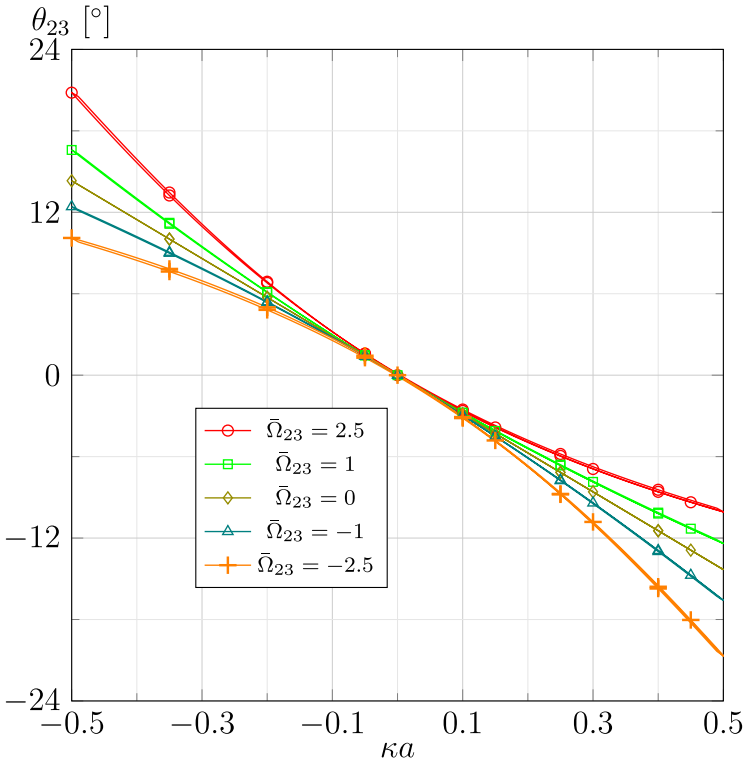

Fig. 7. The average rotation angle θ_{23} (52) in degrees for $r = a$ for different $\bar{\Omega}_{23}$ and cyclic loading with $\kappa a \in [0, 0.5] \cup [0.5, -0.5] \cup [-0.5, 0.5]$.

it follows that

$$\text{curl}^{+}(\mathbf{L}_p^{+}) = \mathbf{Q}\,\text{curl}(\mathbf{L}_p)\,\mathbf{Q}^T\,,$$

which is used to confirm the validity of (19).

Appendix B. The plastic rate in crystal plasticity

Crystal plasticity models rely on a finite number N of slip systems in the crystal, each system I being able to develop a plastic slip rate ${}_I\Gamma$ and characterized by a plane with unit normal ${}_I\mathbf{n}$ and unit slip direction ${}_I\mathbf{s}$ in that plane (e.g. Rice, 1971). Therefore, the plastic rate $\mathbf{L}_p$ is assumed in the form

$$\mathbf{L}_p = \sum_{I=1}^{N} {}_I\Gamma\, {}_I\mathbf{s} \otimes {}_I\mathbf{n}\,. \tag{B.1}$$

Since ${}_I\mathbf{s} \cdot {}_I\mathbf{n} = 0$, Eq. (B.1) for $\mathbf{L}_p$ is applicable to isochoric metal plasticity, being consistent with (15). Also, N and the relative orientations of the slip systems depend on the metal crystallography (see, e.g., Hull and Bacon, 2001, and references therein).

In the Eulerian framework, the elastic distortional microstructural vectors $\mathbf{m}_i'$ in Eq. (12) are used to model crystal plasticity, by specifying (Rubin, 2021, Section 5.13)

$${}_I\mathbf{n} = \frac{{}_In_i\mathbf{m}^{i'}}{|{}_In_j\mathbf{m}^{j'}|}\,, \quad {}_I\mathbf{s} = \frac{{}_Is^i\mathbf{m}_i'}{|{}_Is^j\mathbf{m}_j'|}\,, \quad {}_In_i\,{}_In_i = 1\,, \quad {}_Is^i\,{}_Is^i = 1\,, \quad {}_In_i\,{}_Is^i = 0\,, \tag{B.2}$$

where there is no sum on the repeated index I and the components ${}_In_i$ of ${}_I\mathbf{n}$ and the components ${}_Is^i$ of ${}_I\mathbf{s}$ are constants that are defined in a zero-stress state, where $\mathbf{m}_i' = \mathbf{m}^{i'}$ are orthonormal unit vectors.

Eq. (B.2) simply states that the crystallographic directions follow the crystal lattice, which is subject to elastic deformation.

In contrast to Eq. (27), in the framework of crystal plasticity the plastic spin rate directly comes from Eqs. (26) and (B.1), such as it has the form

$$\mathbf{W}_p = \sum_{I=1}^{N} \frac{{}_I\Gamma}{2}\,({}_I\mathbf{s} \otimes {}_I\mathbf{n} - {}_I\mathbf{n} \otimes {}_I\mathbf{s}). \tag{B.3}$$

Each plastic slip rate ${}_I\Gamma$ in (B.1) typically is a function of history-dependent variables that may have forms similar to that of the Γ function in Eq. (32). Incorporating the smooth elastic–plastic transition has the advantage of avoiding the non-uniqueness in the activation of slip systems that is typical of rate-independent crystal plasticity based on conventional consistency conditions (Gambin, 1992; Forest and Rubin, 2016). Finally, this crystal plasticity formulation is properly invariant under SRBM if ${}_I\Gamma$ are unaffected by SRBM, i.e. ${}_I\Gamma^+ = {}_I\Gamma$.

Data availability

We will share the Mathematica code upon reasonable request.

References

Acharya, A., Bassani, J., 2000. Lattice incompatibility and a gradient theory of crystal plasticity. J. Mech. Phys. Solids 48 (8), 1565–1595. http://dx.doi.org/10.1016/S0022-5096(99)00075-7.

Acharya, A., Zhang, X., 2015. From dislocation motion to an additive velocity gradient decomposition, and some simple models of dislocation dynamics. Chin. Ann. Math. Ser. B 36 (5), 645–658. http://dx.doi.org/10.1007/s11401-015-0970-0.

Arsenlis, A., Parks, D.M., 1999. Crystallographic aspects of geometrically-necessary and statistically-stored dislocation density. Acta Mater. 47 (5), 1597–1611. http://dx.doi.org/10.1016/S1359-6454(99)00020-8.

Asaro, R.J., 1975. Elastic-plastic memory and kinematic-type hardening. Acta Metall. 23, 1255–1265. http://dx.doi.org/10.1016/0001-6160(75)90044-9.

Ashby, M.F., 1970. The deformation of plastically non-homogeneous materials. Phil. Mag. 21, 399–424. http://dx.doi.org/10.1080/14786437008238426.

Bardella, L., 2009. A comparison between crystal and isotropic strain gradient plasticity theories with accent on the role of the plastic spin. Eur. J. Mech. A-Solid. 28 (3), 638–646. http://dx.doi.org/10.1016/j.euromechsol.2008.10.006.

Bardella, L., Panteghini, A., 2015. Modelling the torsion of thin metal wires by distortion gradient plasticity. J. Mech. Phys. Solids 78, 467–492. http://dx.doi.org/10.1016/j.jmps.2015.03.003.

Bassani, J.L., 2001. Incompatibility and a simple gradient theory of plasticity. J. Mech. Phys. Solids 49 (9), 1983–1996. http://dx.doi.org/10.1016/S0022-5096(01)00037-0.

Besseling, J., 1966. A thermodynamic approach to rheology. In: Parkus, H., Sedov, L. (Eds.), Proceedings of the IUTAM Symposium on Irreversible Aspects of Continuum Mechanics and Transfer of Physical Characteristics in Moving Fluids, Vienna. pp. 16–53.

Bilby, B.A., Gardner, L.R.T., Stroh, A.N., 1957. Continuous distributions of dislocations and the theory of plasticity. In: Proceedings of the 9th International Congress of Applied Mechanics, vol. 9, University de Brussels, pp. 35–44.

Bodner, S.R., 1985. Evolution equations for anisotropic hardening and damage of elastic-viscoplastic materials. Plast. Today Model. Methods Appl. 471–482.

Bodner, S.R., Partom, Y., 1972. A large deformation elastic-viscoplastic analysis of a thick-walled spherical shell. J. Appl. Mech.-T ASME 39, 751–757. http://dx.doi.org/10.1115/1.3422784.

Bodner, S.R., Rubin, M.B., 1994. Modeling of hardening at very high strain rates. J. Appl. Phys. 76 (5), 2742–2747. http://dx.doi.org/10.1063/1.357578.

Cermelli, P., Gurtin, M.E., 2001. On the characterization of geometrically necessary dislocations in finite plasticity. J. Mech. Phys. Solids 49 (7), 1539–1568. http://dx.doi.org/10.1016/S0022-5096(00)00084-3.

Chan, K.S., Bodner, S.R., Lindholm, U.S., 1988. Phenomenological modeling of hardening and thermal recovery in metals. J. Eng. Mater.-T ASME 110, 1–8. http://dx.doi.org/10.1115/1.3226003.

Chiricotto, M., Giacomelli, L., Tomassetti, G., 2016. Dissipative scale effects in strain-gradient plasticity: the case of simple shear. SIAM J. Appl. Math. 76 (2), 688–704. http://dx.doi.org/10.1137/15M1048227.

Eckart, C., 1948. The thermodynamics of irreversible processes. IV. The theory of elasticity and anelasticity. Phys. Rev. 73, 373–382. http://dx.doi.org/10.1103/PhysRev.73.373.

El-Naaman, S., Nielsen, K., Niordson, C., 2019. An investigation of back stress formulations under cyclic loading. Mech. Mater. 130, 76–87. http://dx.doi.org/10.1016/j.mechmat.2019.01.005.

Fleck, N.A., Hutchinson, J.W., 1997. Strain gradient plasticity. Adv. Appl. Mech. 33, 295–361.

Fleck, N.A., Hutchinson, J.W., Willis, J.R., 2014. Strain gradient plasticity under non-proportional loading. Proc. R. Soc. A 470, 20140267. http://dx.doi.org/10.1098/rspa.2014.0267.

Fleck, N.A., Muller, G.M., Ashby, M.F., Hutchinson, J.W., 1994. Strain gradient plasticity: theory and experiments. Acta Metall. Mater. 42, 475–487. http://dx.doi.org/10.1016/0956-7151(94)90502-9.

Forest, S., Rubin, M., 2016. A rate-independent crystal plasticity model with a smooth elastic-plastic transition and no slip indeterminacy. Eur. J. Mech. A-Solid. 55, 278–288. http://dx.doi.org/10.1016/j.euromechsol.2015.08.012.

Fosdick, R., Royer-Carfagni, G., 2020. Hadamard's conditions of compatibility from Cesaro's line-integral representation. Internat. J. Engrg. Sci. 146, 103174. http://dx.doi.org/10.1016/j.ijengsci.2019.103174.

Gambin, W., 1992. Refined analysis of elastic-plastic crystals. Int. J. Solids Struct. 29, 2013–2021. http://dx.doi.org/10.1016/0020-7683(92)90191-U.

Green, A.E., Naghdi, P.M., 1965. A general theory of an elastic-plastic continuum. Arch. Ration. Mech. An. 18, 251–281. http://dx.doi.org/10.1007/BF00251666.

Greer, J.R., De Hosson, J.T., 2011. Plasticity in small-sized metallic systems: Intrinsic versus extrinsic size effect. Prog. Mater. Sci. 56 (6), 654–724. http://dx.doi.org/10.1016/j.pmatsci.2011.01.005.

Gudmundson, P., 2004. A unified treatment of strain gradient plasticity. J. Mech. Phys. Solids 52, 1379–1406. http://dx.doi.org/10.1016/j.jmps.2003.11.002.

Gurtin, M.E., 2004. A gradient theory of small-deformation isotropic plasticity that accounts for the Burgers vector and for dissipation due to plastic spin. J. Mech. Phys. Solids 52, 2545–2568. http://dx.doi.org/10.1016/j.jmps.2004.04.010.

Hollenstein, M., Jabareen, M., Rubin, M.B., 2013. Modeling a smooth elastic–inelastic transition with a strongly objective numerical integrator needing no iteration. Comput. Mech. 52, 649–667. http://dx.doi.org/10.1007/s00466-013-0838-7.

Hollenstein, M., Jabareen, M., Rubin, M.B., 2015. Erratum to: Modeling a smooth elastic–inelastic transition with a strongly objective numerical integrator needing no iteration. Comput. Mech. 55, 453. http://dx.doi.org/10.1007/s00466-014-1099-9.

Huang, Y., Gao, H., Nix, W.D., Hutchinson, J.W., 2000. Mechanism-based strain gradient plasticity — II. Analysis. J. Mech. Phys. Solids 48, 99–128. http://dx.doi.org/10.1016/S0022-5096(99)00022-8.

Hull, D., Bacon, D., 2001. Introduction to dislocations, fourth ed. Butterworth-Heinemann, Oxford.

Hwang, K.C., Jiang, H., Huang, Y., Gao, H., 2003. Finite deformation analysis of mechanism-based strain gradient plasticity: torsion and crack tip field. Int. J. Plast. 19, 235–251. http://dx.doi.org/10.1016/S0749-6419(01)00039-0.

Johnson, J., Barker, L., 1969. Dislocation dynamics and steady plastic wave profiles in 6061-T6 aluminum. J. Appl. Phys. 40 (11), 4321–4334. http://dx.doi.org/10.1063/1.1657194.

Kiener, D., Motz, C., Grosinger, W., Weygand, D., Pippan, R., 2010. Cyclic response of copper single crystal micro-beams. Scripta Mater. 63 (5), 500–503. http://dx.doi.org/10.1016/j.scriptamat.2010.05.014.

Kröner, E., 1959. General continuum theory of dislocations and intrinsic stresses. Arch. Ration. Mech. An. 4, 273–334. http://dx.doi.org/10.1007/BF00281393.

Kröner, E., 1962. Dislocations and continuum mechanics. Appl. Mech. Rev. 15, 599–606.

Lee, E.H., 1969. Elastic-plastic deformation at finite strains. J. Appl. Mech. 36, 1–6. http://dx.doi.org/10.1115/1.3564580.

Lee, E.H., Rubin, M.B., 2021. Modeling inelastic spin of microstructural vectors in sheet metal forming. Int. J. Solids Struct. 225, 111067. http://dx.doi.org/10.1016/j.ijsolstr.2021.111067.

Leonov, A.I., 1976. Nonequilibrium thermodynamics and rheology of viscoelastic polymer media. Rheol. Acta 15, 85–98. http://dx.doi.org/10.1007/BF01517499.

Liu, D., He, Y., Dunstan, D.J., Zhang, B., Gan, Z., Hu, P., Ding, H., 2013. Anomalous plasticity in cyclic torsion of micron scale metallic wires. Phys. Rev. Lett. 110, 244301. http://dx.doi.org/10.1103/PhysRevLett.110.244301.

Malvern, L.E., 1951. The propagation of longitudinal waves of plastic deformation in a bar of material exhibiting a strain-rate effect. J. Appl. Mech.-T ASME 18, 203–208.

Needleman, A., 2024. A perspective on plasticity, dissipation and the second law of thermodynamics. J. Appl. Mech.-T ASME 91 (6), 061003. http://dx.doi.org/10.1115/1.4064700.

Niordson, C.F., Hutchinson, J.W., 2003. On lower order strain gradient plasticity theories. Eur. J. Mech. A-Solid. 22 (6), 771–778. http://dx.doi.org/10.1016/S0997-7538(03)00069-X.

Nye, J.F., 1953. Some geometrical relations in dislocated crystals. Acta Metall. 1, 153–162. http://dx.doi.org/10.1016/0001-6160(53)90054-6.

Onat, E., 1968. The notion of state and its implications in thermodynamics of inelastic solids. In: Irreversible Aspects of Continuum Mechanics and Transfer of Physical Characteristics in Moving Fluids: Symposia Vienna, June 22–28, 1966. pp. 292–314.

Panteghini, A., Bardella, L., 2020. Modelling the cyclic torsion of polycrystalline micron-sized copper wires by distortion gradient plasticity. Phil. Mag. 100 (18), 2352–2364. http://dx.doi.org/10.1080/14786435.2020.1766144.

Perzyna, P., 1963. The constitutive equations for rate sensitive plastic materials. Quart. Appl. Math. 20, 321–332. http://dx.doi.org/10.1090/qam/144536.

Proudhon, H., Poole, W., Wang, X., Bréchet, Y., 2008. The role of internal stresses on the plastic deformation of the Al-Mg-Si-Cu alloy AA6111. Phil. Mag. 88 (5), 621–640. http://dx.doi.org/10.1080/14786430801894569.

Reynolds, A., Baxter, S., 2000. Kinematic hardening in a dispersion strengthened aluminum alloy: experiment and modeling. Mater. Sci. Eng./A 285 (1), 265–279. http://dx.doi.org/10.1016/S0921-5093(00)00645-6.

Rice, J.R., 1971. Inelastic constitutive relations for solids: an internal-variable theory and its application to metal plasticity. J. Mech. Phys. Solids 19 (6), 433–455. http://dx.doi.org/10.1016/0022-5096(71)90010-X.

Rubin, M.B., 1994. Plasticity theory formulated in terms of physically based microstructural variables – Part I. Theory. Int. J. Solids Struct. 31, 2615–2634. http://dx.doi.org/10.1016/0020-7683(94)90222-4.

Rubin, M.B., 2012. Removal of unphysical arbitrariness in constitutive equations for elastically anisotropic nonlinear elastic–viscoplastic solids. Internat. J. Engrg. Sci. 53, 38–45. http://dx.doi.org/10.1016/j.ijengsci.2011.12.008.

Rubin, M.B., 2021. Continuum Mechanics with Eulerian Formulations of Constitutive Equations. Springer Nature.

Rubin, M.B., Attia, A.V., 1996. Calculation of hyperelastic response of finitely deformed elastic-viscoplastic materials. Int. J. Num. Meth. Eng. 39, 309–320. http://dx.doi.org/10.1002/(SICI)1097-0207(19960130)39:2<309::AID-NME858>3.0.CO;2-B.

Rubin, M., Bardella, L., 2023. An Eulerian thermodynamical formulation of size-dependent plasticity. J. Mech. Phys. Solids 170, 105122. http://dx.doi.org/10.1016/j.jmps.2022.105122.

Sadik, S., Yavari, A., 2017. On the origins of the idea of the mulctiplicative decomposition of the deformation gradient. Math. Mech. Solids 22 (4), 771–772. http://dx.doi.org/10.1177/1081286515612280.

Shizawa, K., Zbib, H., 1999. A thermodynamical theory of gradient elastoplasticity with dislocation density tensor. I: Fundamentals. Int. J. Plast. 15 (9), 899–938. http://dx.doi.org/10.1016/S0749-6419(99)00018-2.

Starkey, K., Winther, G., El-Azab, A., 2020. Theoretical development of continuum dislocation dynamics for finite-deformation crystal plasticity at the mesoscale. J. Mech. Phys. Solids 139, 103926. http://dx.doi.org/10.1016/j.jmps.2020.103926.

Stoltz, R.E., Pelloux, R.M., 1976. The Bauschinger effect in precipitation strengthened aluminum alloys. Metall. Trans. A 7, 1295–1306. http://dx.doi.org/10.1007/BF02658814.

Stout, M.G., Rollett, A.D., 1990. Technical Report LA-UR-90-572. Los Alamos.

Taillard, R., Pineau, A., 1982. Room temperature tensile properties of Fe-19wt.%Cr alloys precipitation hardened by the intermetallic compound NiAl. Mater. Sci. Eng. 56 (3), 219–231. http://dx.doi.org/10.1016/0025-5416(82)90097-0.

Wilkinson, A.J., Meaden, G., Dingley, D.J., 2006. High-resolution elastic strain measurement from electron backscatter diffraction patterns: New levels of sensitivity. Ultramicroscopy 106 (4–5), 307–313. http://dx.doi.org/10.1016/j.ultramic.2005.10.001.

Willis, J.R., 1967. Second-order effects of dislocations in anisotropic crystals. Internat. J. Engrg. Sci. 5, 171–190. http://dx.doi.org/10.1016/0020-7225(67)90003-1.

Wulfinghoff, S., Forest, S., Böhlke, T., 2015. Strain gradient plasticity modelling of the cyclic behaviour of laminate microstructures. J. Mech. Phys. Solids 79, 1–20. http://dx.doi.org/10.1016/j.jmps.2015.02.008.

Yavari, A., 2013. Compatibility equations of nonlinear elasticity for non-simply-connected bodies. Arch. Ration. Mech. An. 209, 237–253. http://dx.doi.org/10.1007/s00205-013-0621-0.